BROADBAND LOADED DIPOLE ANTENNA DESIGN BY GENETIC ALGORITHM OPTIMIZATION

A THESIS SUBMITTED TO
THE GRADUATE SCHOOL OF NATURAL AND APPLIED SCIENCES
OF
MIDDLE EAST TECHNICAL UNIVERSITY

BY

BAHRI ASAN

IN PARTIAL FULFILLMENT OF THE REQUIREMENTS
FOR
THE DEGREE OF MASTER OF SCIENCE
IN
ELECTRICAL AND ELECTRONICS ENGINEERING

FEBRUARY 2014

Approval of the thesis:

BROADBAND LOADED DIPOLE ANTENNA DESIGN BY GENETIC ALGORITHM OPTIMIZATION

submitted by **BAHRI ASAN** in partial fulfillment of the requirements for the degree of **Master of Science in Electrical and Electronics Engineering Department, Middle East Technical University** by,

Prof. Dr. Canan Özgen _____
Dean, Graduate School of **Natural and Applied Sciences**

Prof. Dr. Gönül Turhan Sayan _____
Head of Department, **Electrical and Electronics Eng.**

Prof. Dr. Sencer Koç _____
Supervisor, **Electrical and Elect. Eng. Dept., METU**

Examining Committee Members:

Prof. Dr. Nilgün Günalp
Electrical and Electronics Engineering Department, METU _____

Prof. Dr. Sencer Koç
Electrical and Electronics Engineering Department, METU _____

Prof. Dr. Özlem Çivi Aydın
Electrical and Electronics Engineering Department, METU _____

Assoc. Prof. Dr. Lale Alatan
Electrical and Electronics Engineering Department, METU _____

Assoc. Prof. Dr. Vakur Ertürk
Electrical and Electronics Engineering Department,
Bilkent University _____

Date: _____

I hereby declare that all information in this document has been obtained and presented in accordance with academic rules and ethical conduct. I also declare that, as required by these rules and conduct, I have fully cited and referenced all material and results that are not original to this work.

Name, Last Name: BAHRI ASAN

Signature :

ABSTRACT

BROADBAND LOADED DIPOLE ANTENNA DESIGN BY GENETIC ALGORITHM OPTIMIZATION

ASAN, BAHRi

M.S., Department of Electrical and Electronics Engineering

Supervisor : Prof. Dr. Sencer Koç

February 2014, 90 pages

It is well known that standard dipole antenna is not convenient to be used in broadband wireless communication applications because of its narrow frequency bandwidth. To broaden the bandwidth of a dipole, lumped loading is the generally applied method. Positive effects of resistive, capacitive and inductive loading are discussed and proved for a pretty long time.

This thesis investigates broadband lumped loaded dipole antenna design procedure by using genetic algorithm optimization techniques. First, unloaded dipole antenna numerical analysis formulation is provided by EFIE (Electric Field Integral Equation) derivation. MoM (Method of Moments) is used for numerical solution. Then, analysis is extended for lumped loaded dipole antenna. Analysis computer code is developed in MATLAB environment and results are compared with NEC (Numerical Electromagnetic Code). To design loaded dipole antenna with corresponding matching network which satisfies the predefined ra-

diation parameters, genetic algorithm (GA) optimization methods are used . GA searches for an optimal solution from random solution set with iterative methods. Optimization objectives are selected as increasing the minimum antenna gain and decreasing the maximum VSWR. Load values, positions and matching network variables are optimized simultaneously. Finally, successfully optimized broadband loaded dipole antenna and matching network design examples are presented to verify the used procedure.

Keywords: Loaded Dipole Antenna, Genetic Algorithm, EFIE, Broadband Antenna, Optimization, Matching Network

ÖZ

GENETİK ALGORİTMA OPTİMİZASYONU İLE GENİŞ BANTLI DİPOL ANTEN TASARIMI

ASAN, BAHRi
Yüksek Lisans, Elektrik ve Elektronik Mühendisliği Bölümü
Tez Yöneticisi : Prof. Dr. Sencer Koç

Şubat 2014 , 90 sayfa

Dipol antenlerin dar frekans bantlarından dolayı genişbant kablosuz haberleşme uygulamalarına uygun olmadığı bilinmektedir. Dipol antenin bantgenişliğini artırmak için genellikle yükleme metodu kullanılır. Direnç, kapasitör ve indüktör ile yapılan anten yüklemelerinin olumlu etkileri uzun zamandır tartışılmış ve kanıtlanmıştır.

Bu tezde, "Genetik Algoritma" optimizasyon metoduyla genişbant yüklü dipol anten tasarım prosedürü incelenmiştir. Öncelikle yüksüz dipol anten için nümerik analiz formülasyonu "Elektrik Alan İntegral Denklemi" nin çözümüyle elde edilmiştir. Nümerik çözüm için "Moment Metod" yöntemi kullanılmıştır. Daha sonra analiz, yüklü anten için genişletilmiştir. Analiz kodu, MATLAB ortamında geliştirilmiş ve sonuçlar "NEC (Nümerik Elektromanyetik Kod)" sonuçları ile karşılaştırılmıştır. Önceden belirlenmiş parametreleri sağlayacak şekilde yüklü dipol anten ve uyumlama devresi tasarımı genetik algoritma optimizas-

yon metodları kullanılarak yapılmıştır. Genetik algoritma rastgele bir çözüm kümesinden en uygun sonucu yinelemeli metodlarla arar. Optimizasyon hedefleri minimum anten kazançını artırmak ve maksimum VSWR değerini azaltmak olarak belirlenmiştir. Yüklerin değerleri, pozisyonları ve uyumlama devresi elemanları eşzamanlı olarak optimize edilmiştir. Son olarak, kullanılan yöntemi doğrulamak için başarılı bir şekilde optimize edilmiş genişband yüklü anten ve uyumlama devresi tasarım örnekleri gösterilmiştir.

Anahtar Kelimeler: Yüklü Dipol Anten, Genetik Algoritma, Genişbantlı Anten, Optimizasyon, Uyumlama Devresi

To my wife

Tuğba

ACKNOWLEDGMENTS

I would like to thank my supervisor Professor Sencer Koç for his support and guidance through out the thesis study.

I am also grateful to Turkish Air Force Electronic Warfare Support Center (EHDM) staff, my colleagues and friends. Especially to my manager Major Alparslan Türkboyları for his insightfullness and also to my friends Captain Osman Coşkun and Lieutenant Kadir Keskin for his help in writing this report and Captain Hakan Abacı for his guidance.

I wish also thank to my parents Hasan Asan, Şengül Asan and my little sister Büşra Asan for encouragement that they provided to me.

Finally, I would like to express my deepest gratitude to my wife, Tuğba Asan for her endless patience, support and clemency not only for this thesis work, for our whole marriage.

TABLE OF CONTENTS

LIST OF FIGURES

FIGURES

CHAPTER 1

INTRODUCTION

Dipole antennas are widely used in wireless systems especially in mobile communication and TV-radio broadcasting. Its linear polarization and omnidirectional radiation pattern in azimuth, provides an advantage to be used extensively. However with the recent multi-band and broadband applications, communication antennas are required to be operated in wide frequency ranges. This may restrict the usage of dipoles since they are inherently narrowband antennas.

Bandwidth of a narrowband antenna is expressed as percentage of the frequency difference (upper minus lower) over the center frequency. However for broadband antennas, usually the ratio of upper to lower frequency of operation is used to express bandwidth [1]. If we define f_U as the upper frequency and f_L as the lower frequency of operation, bandwidth for broadband antennas is defined as B_r by [22]

$$B_r = \frac{f_U}{f_L}$$

An antenna can be classified as broadband if the input impedance and the pattern of the antenna do not change significantly over about an octave (f_U/f_L=2) or more and satisfy the criteria [22].

In most cases VSWR and the gain are the parameters that determine the antenna bandwidth. According to [10] an antenna can be defined as operational at frequencies where the return loss (RL), is sufficiently small (below -10 dB) if the antenna gain is acceptable. It corresponds to a VSWR about 2. Collin also gives acceptable VSWR limit as 1.5 [4].

Figure (1.1), which is drawn by the use of NEC data, represents the VSWR behavior of a 30 cm dipole antenna over the frequencies from half-wavelength ($\lambda/2$) to two wavelengths (2λ). As shown, VSWR of the dipole antenna is acceptable only where the antenna becomes half-wavelength ($\lambda/2$) and 1.5 wavelength ($3\lambda/2$). That's why dipole antennas are classified as narrowband antennas.

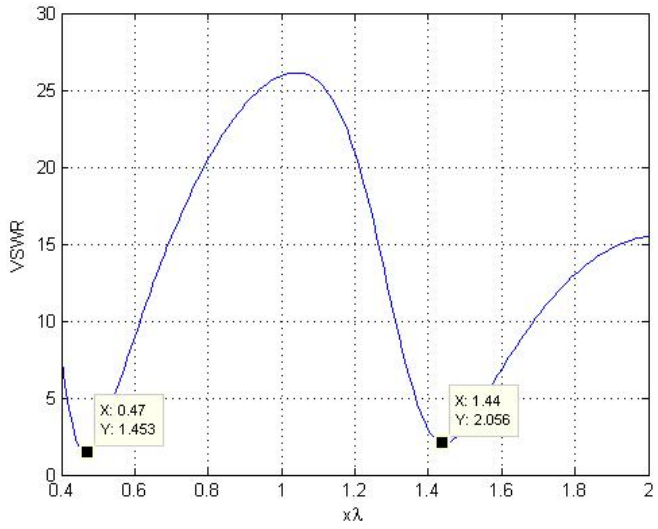

Figure 1.1: VSWR of 30 cm Dipole Antenna, drawn by the use of NEC Data

The reason of this narrowband behavior is the reflections from the ends of the dipole antenna [10]. To prevent end reflections, a variable internal impedance per unit length was introduced to the antenna by Wu and King [23]. This approach is successful in providing linear current distribution over the antenna, almost independent of frequency. To obtain the same result with negligible losses, Hallen [6] modified this approach by using variable capacitance instead of impedance. Several resistive, capacitive and inductive loading investigations have been done to broaden the bandwidth of the dipole and monopole antennas [8, 11, 16].

Lumped loading is an alternative method to distributed loading. It causes smaller ohmic losses since small number of loads are used. It has been shown in several studies that resistive, capacitive and/or inductive lumped loading of dipole and monopole antennas can provide the broadband operation [2, 5]. However, lumped loading requires an optimization process for the appropriate

locations of the loading and the load values.

With the advent of genetic algorithm, it is applied in several antenna loading studies and has been demonstrated to be a powerful tool for the loaded wire antenna design [7]. Parallel R-L-C load positions and the values over a monopole and also a matching network was optimized successfully in [2]. R-L circuit was loaded to satisfy 5:1 and 20:1 bandwidth for monopole antenna in [18]. L-C circuit loading was investigated in [5].

1.1 Outline of the Thesis

The problem, considered in this thesis work is the design of a loaded dipole antenna and a corresponding matching network that satisfy the predefined VSWR and antenna gain requirements over a broad frequency band. Antennas with bandwidth ratio of 2:1 and more are accepted as broadband antennas according to [22].

First of all, unloaded dipole antenna analysis is investigated in Chapter 2. A MATLAB code is written which calculates the dipole antenna radiation parameters; antenna gain, input impedance, reflection loss and VSWR.

Dipole antennas are modeled as strips. Strip antenna modeling is based on the assumption that a thin wire antenna with a non-circular cross section behaves like a cylindrical antenna of an equivalent radius [10, 22]. This 2D modeling provides simplicity during construction of the antenna and the establishment of the formulation. Concerns about the reliability of the formulation, because of the loss of one dimension, are eliminated by comparing the results with Numerical Electromagnetic Code (NEC) [3] results.

To analyze the dipole antenna, EFIE (Electric Field Integral Equation) formulation is used. EFIE is based on the boundary condition of the total tangential electric field, which yields an integral equation that involves induced current density as a part of integrand. Once the current density is solved, other antenna parameters are easily calculated [1].

EFIE is numerically solved by the use of Method of Moments (MoM). MoM provides a solution of EFIE by expanding the unknown function (surface current density for antenna radiation) as a linear combination of known functions, with unknown coefficients. Then, equation is converted to matrix form and unknown coefficients are calculated by the use of matrix algebra.

After the formulation for unloaded dipole antenna radiation is established, analysis is extended for lumped loaded dipole antenna in Chapter 3. Lumped loading is implemented by the modification of boundary condition only at the load positions. By the use of method suggested in [10], effects of the loads are included to the general formulation easily by adjusting only the related parts. Moreover, a matching network that consists of a transformer and a parallel inductance as suggested in [19] is also implemented in this part.

By the end of Chapter 3, formulation for antenna gain, input impedance and VSWR have been provided for an arbitrarily loaded dipole antenna and corresponding matching network over a predetermined frequency band. Results of the MATLAB code and the NEC are compared for unloaded and loaded dipole antennas with different configurations.

In Chapter 4, "Genetic Algorithm" optimization procedure and implementation of optimization to lumped loaded dipole antenna is investigated. A computer program is developed to optimize a loaded dipole antenna and a matching network simultaneously that satisfy the predetermined antenna parameters. This program uses the results of the program developed in the first part as input to achieve the optimization.

Objectives of the optimization are decided as maximizing the minimum forward gain and minimizing the maximum VSWR over a broadband frequency. Antenna size, load counts, load value limits and operational frequency range are selectable by the user.

At the end, several optimization examples are done to achieve 4.5:1 bandwidth over 400-1800 MHz and 5:1 bandwidth over 400-2000 MHz with 30 cm length loaded dipole antenna. Requirements are decided as minimum -3 dB of system

gain and maximum VSWR of 3.5 to be parallel with previous studies [2, 5, 18, 19]. 3 parallel R-L-C circuits are used as loads and matching network is composed of a parallel inductance and a transformer.

CHAPTER 2

DIPOLE ANTENNA ANALYSIS

This chapter covers the unloaded dipole antenna analysis. In the first section EFIE is derived and numerical methods for its solutions are introduced. Then, formulation for the radiation parameters of the unloaded antenna is provided in the second section.

2.1 EFIE Derivation

EFIE derivation is based on the following boundary condition; when the antenna is excited by an incident field $\overline{E}^i$, surface currents distribute themselves such that the total tangential electric field $\overline{E}^{total}$ on the antenna is zero

$$\widehat{n} \times \overline{E}^{total}(r = r_s) = 0$$

where r_s represent the points on the antenna surface.

When a conductor exists, total electric field can be written as summation of the incident and the scattered electric fields:

$$\overline{E}^{total}(r) = \overline{E}^i(r) + \overline{E}^s(r).$$

Then, boundary condition on the antenna surface can be defined as:

$$\begin{aligned} \widehat{n} \times \overline{E}^{total}(r = r_s) &= \widehat{n} \times (\overline{E}^i(r = r_s) + \overline{E}^s(r = r_s)) = 0 \\ \widehat{n} \times \overline{E}^i(r = r_s) &= -\widehat{n} \times \overline{E}^s(r = r_s)). \end{aligned} \tag{2.1}$$

In general the scattered electric field ($\overline{E}^s$) generated by the induced surface current density ($\overline{J}$) is given by [1]:

$$\overline{E}^s = -j\omega\overline{A} - \nabla\Phi$$

where $\overline{A}$ is the magnetic vector potential and Φ is the scalar electric potential.

For observation points on the antenna surface, we are interested only in the tangential components:

$$\overline{E}_t^s = -j\omega\overline{A}_t - \nabla_t\Phi \tag{2.2}$$

where subscript "t" denotes the tangential component. Vector potential and scalar potential, by the use of "Continuity Equation", can be written as:

$$\begin{aligned}
\overline{A}_t(r) &= \frac{\mu}{4\pi}\int_s \overline{J}(r')\frac{e^{-jkR}}{R}ds' \\
\Phi(r) &= \frac{1}{4\pi\epsilon}\int_s \sigma(r')\frac{e^{-jkR}}{R}ds' \\
\nabla\cdot\overline{J} &= -j\omega\sigma \\
\Phi(r) &= -\frac{1}{j\omega\epsilon 4\pi}\int_s \nabla\cdot\overline{J}(r')\frac{e^{-jkR}}{R}ds'
\end{aligned}$$

where σ is the surface charge density, r is the observation point, r' is the source point and R is the distance between the source and the observation points, $R = |r - r'|$.

Then, tangential $\overline{E}_t^s$ field can be written as:

$$\overline{E}_t^s(r) = -\frac{j\omega\mu}{4\pi}\int_s \overline{J}(r')\frac{e^{-jkR}}{R}ds' + \frac{1}{j\omega\epsilon 4\pi}\int_s \nabla_t(\nabla\cdot\overline{J}(r'))\frac{e^{-jkR}}{R}ds'.$$

Since tangential scattered electric field $\overline{E}_t^s$ on the antenna surface is known by the use of (2.1), we can locate our observation point "r" on the antenna surface;

$$\begin{aligned}
\overline{E}_t^s(r = r_s) &= -\overline{E}_t^i(r = r_s) \\
\overline{E}_t^i(r = r_s) &= \frac{j\omega\mu}{4\pi}\int_s \overline{J}(r')\frac{e^{-jkR}}{R}ds' - \frac{1}{j\omega\epsilon 4\pi}\int_s \nabla_t(\nabla\cdot\overline{J}(r'))\frac{e^{-jkR}}{R}ds'
\end{aligned} \tag{2.3}$$

Left hand side of equation (2.3) will be non-zero only at the source region, since $\overline{E}^i$ incident field exist only there. When "r" is selected out of the source region, equation will be equal to zero.

2.1.1 Antenna Model

In this study, dipole antennas are modeled as rectangular, two dimensional strips. A circular dipole with radius "a" is replaced with an equivalent strip of "a_{eqv}" width. Equivalence will be discussed in the corresponding Section (3.3.4). Strips are located on the $(x-z)$ plane and length of dipole is oriented to the z axis. Hence, antenna has been positioned between the points $(\frac{\pm a_{eqv}}{2}, 0, 0)$ and $(\frac{\pm a_{eqv}}{2}, 0, l)$ as shown in Figure (2.1). Feed point coordinate is $(0, 0, \frac{l}{2})$ for center fed dipole.

To solve the integral equation (2.3), which is called EFIE, for surface current density $(\overline{J}_s)$ numerically; integral domain, which is the antenna surface, should be divided into smaller parts. Then, integral will operate on these smaller parts individually and contributions from all parts will be added. Division of the antenna surface into smaller parts is called "Mesh Generation". In this study, triangular mesh generation is used. Triangular mesh model is the most widely used model in antenna analysis applications, since it conforms to any geometrical surface and permits the simple description of the surface and patches to the computer [17]. Antenna surface is divided into planar triangular patches as shown in Figure (2.1).

2.1.2 RWG Basis Functions

The EFIE equation of (2.3) is solved numerically by the use of Method of Moments (MoM). MoM suggests to divide the unknown $\overline{J}_s$ into "n" known functions, which is called basis function, with unknown coefficients. Then, surface current density will be expressed by the use of these coefficients and the basis functions.

Basis function in a problem should be chosen to best represent the unknown.

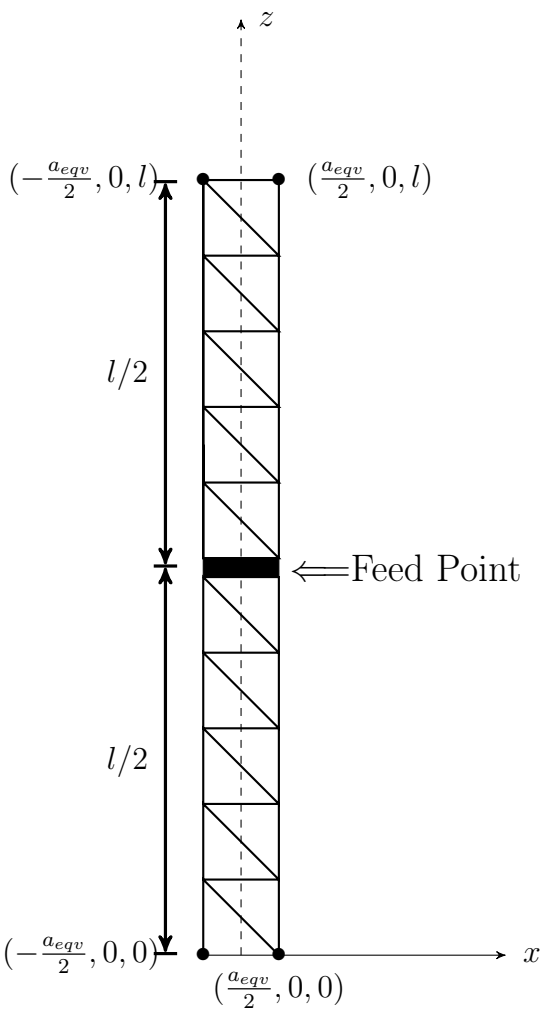

Figure 2.1: Strip Antenna Mesh Model

RWG (Rao-Wilton-Glisson) basis functions have been proven to be useful in antenna radiation problems. The fact that make RWG basis functions valuable is that they allow smooth current density at the edges and eliminate the fictitious charges at the basis elements [17]. RWG basis functions are used in this study, since it successfully represents the current over the antenna.

RWG basis function ($\overline{f}_n$) is defined over two triangles and a common edge.

$$\overline{f_n}(r) = \begin{cases} \frac{l_n}{2A_n^+}\overline{\rho}_n^+(r), & \text{r in } T_n^+ \\ \frac{l_n}{2A_n^-}\overline{\rho}_n^-(r), & \text{r in } T_n^- \\ 0 & otherwise \end{cases}$$

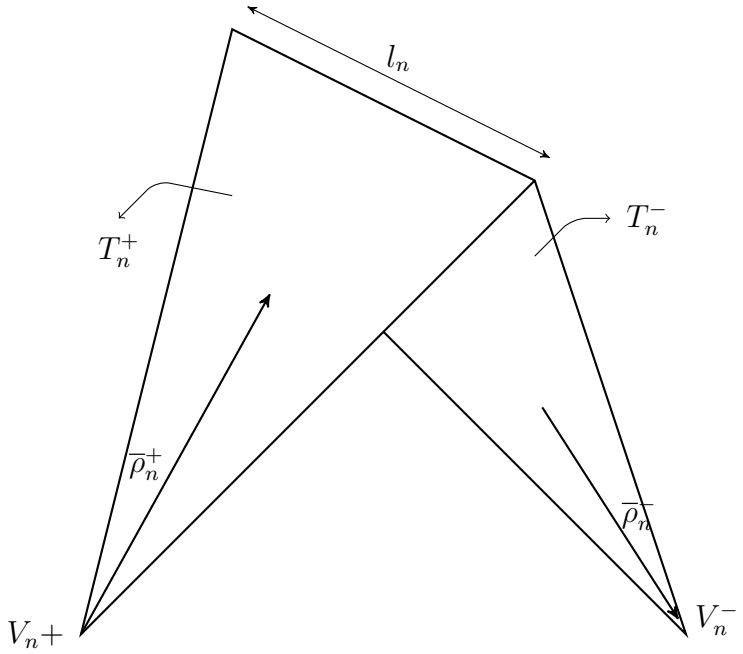

Figure 2.2: RWG Basis Function

RWG basis function is defined on triangular patches, that are obtained by triangular mesh generation. Every non-boundary edge and two triangles surrounding this edge are named as RWG element which is shown in Figure 2.2. Since triangles more then one edges, every triangle may be a part of more then one RWG element. Triangles are named plus (T_n^+) and minus (T_n^-) assuming that current flow is from plus triangle to minus. A_n^+ and A_n^- are the areas of the plus and minus triangles, respectively and l_n is the common edge length. $\overline{\rho}_n^+(r)$ is the vector defined from free vertex of the (T_n^+) triangle to the source point "r" and $\overline{\rho}_n^-(r)$ is the vector defined from source point "r" to free vertex of the triangle (T_n^-).

By the use of RWG basis expansion the surface electric current on the antenna surface is expressed as the sum of the contributions over all edge elements with unknown coefficients as:

$$\overline{J}(r) \;=\; \sum_{n=1}^{N} I_n \overline{f_n}(r)$$

where $\overline{f_n}(r)$ represents the RWG basis function and I_n represents the unknown coefficients [10].

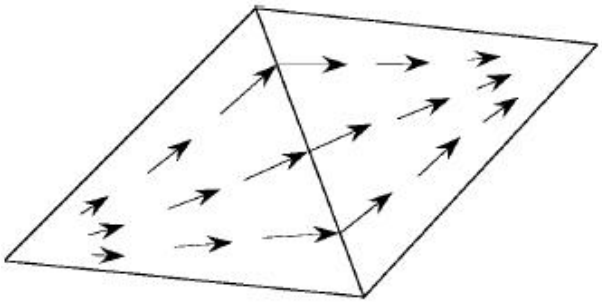

Figure 2.3: RWG Current Flow

The properties of RWG basis functions that give rise to a very good representation of the current that flow on the antenna surface are listed below [17]:

i) RWG functions do not allow current to have component normal to the edges other than the common edge of the RWG element. Basis functions have only tangential components to the other edges, which means no current flows into the non-common edges ($\nabla \cdot \overline{J} = 0$). This implies that there will be no line charges along these edges (except common edge) since, according to the continuity equation, $\nabla \cdot \overline{J} = -j\omega\sigma$.

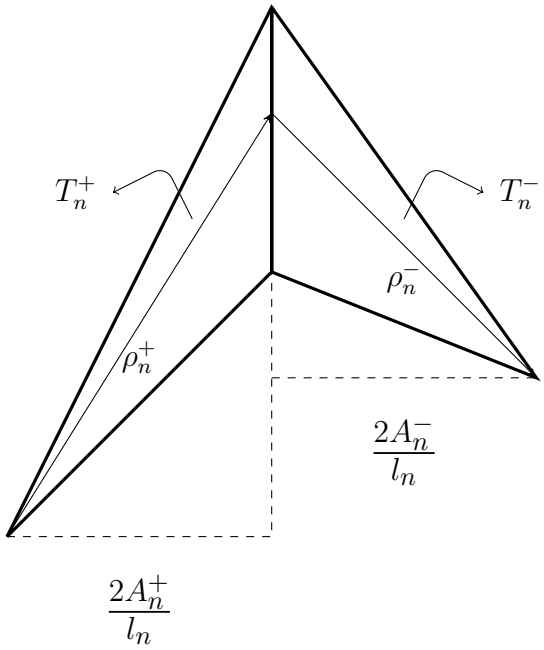

Figure 2.4: RWG Basis Function

ii) RWG basis functions allow the normal component of the current along the common edge to be continuous. As seen in the Figure 2.4, normal component of $\overline{f}_n$ is $\frac{2A_n^{\pm}}{l_n}$ which is just the height of the RWG triangles $T_n^{\pm}$ with common edge. If we normalize $\overline{f}_n$ with $\frac{l_n}{2A_n^{\pm}}$ in $T_n^{\pm}$ respectively, normal components become unit vectors with the same direction. This satisfies the continuity of current normal to the common edge and artificial line charges at the common edge are avoided. Furthermore, since the normal component of the basis function $\overline{f}_n$ at the n_{th} edge is unity, each coefficient I_n may be interpreted as normal component of the current density flowing past the n_{th} edge [17].

iii) The divergence of $\overline{f}_n$ is proportional to the charge density and can be calculated as [17]:

$$\nabla \cdot \overline{f}_n = \begin{cases} \frac{l_n}{A_n^+}, & \text{,r in } T_n^+ \\ -\frac{l_n}{A_n^-}, & \text{,r in } T_n^- \\ 0, & \text{otherwise} \end{cases} \tag{2.4}$$

which means charge density is constant on the triangles $T_n^{\pm}$ and the total charge associated with one triangle pair is zero.

When RWG basis functions are applied, vector potential is obtained as:

$$\begin{aligned} \overline{J}(r') &= \sum_{n=1}^{N} I_n \overline{f}_n(r') \\ \overline{A}(r) &= \frac{\mu}{4\pi} \sum_{n=1}^{N} I_n \int_s \overline{f}_n(r') \frac{e^{-jkR}}{R} ds' \\ \overline{A}(r) &= \frac{\mu}{4\pi} \sum_{n=1}^{N} I_n \left(\int_{T_n^+} \frac{l_n}{2A_n^+} \overline{\rho}_n^+(r') \frac{e^{-jk|r-r'|}}{|r-r'|} ds' + \int_{T_n^-} \frac{l_n}{2A_n^-} \overline{\rho}_n^-(r') \frac{e^{-jk|r-r'|}}{|r-r'|} ds' \right) \end{aligned} \tag{2.5}$$

If we also simplify $\nabla \cdot \overline{f_n}$ by using (2.4), scalar potential can be defined as:

$$\begin{aligned} \Phi(r) &= -\frac{1}{j\omega\epsilon 4\pi} \sum_{n=1}^{N} I_n \int_s \nabla \cdot \overline{f_n}(r') \frac{e^{-jkR}}{R} ds' \\ \Phi(r) &= -\frac{1}{j\omega\epsilon 4\pi} \sum_{n=1}^{N} I_n \left(\int_{T_n^+} \frac{l_n}{A_n^+} \frac{e^{-jk|r-r'|}}{|r-r'|} ds' - \int_{T_n^-} \frac{l_n}{A_n^-} \frac{e^{-jk|r-r'|}}{|r-r'|} ds' \right) \end{aligned} \tag{2.6}$$

At an observation point "r", vector potential $\overline{A}(r)$ and scalar potential $\Phi(r)$ are

expressed as sum of "N" RWG integrals, defined on "N" edges. Therefore, $\overline{E}_t^i$ can be expressed in the same manner by combining (2.5) and (2.6).

$$\begin{aligned}
\overline{E}_t^i(r) &= \frac{j\omega\mu}{4\pi}\sum_{n=1}^{N} I_n \int_s \overline{f}_n(r')\frac{e^{-jkR}}{R}ds' - \frac{1}{j\omega\epsilon 4\pi}\sum_{n=1}^{N} I_n \nabla_t \int_s \nabla\cdot\overline{f}_n(r')\frac{e^{-jkR}}{R}ds' \\
&= \frac{j\omega\mu}{4\pi}\sum_{n=1}^{N} I_n \left(\int_{T_n^+} \frac{l_n}{2A_n^+}\overline{\rho}_n^+(r')\frac{e^{-jk|r-r'|}}{|r-r'|}ds' + \int_{T_n^-} \frac{l_n}{2A_n^-}\overline{\rho}_n^-(r')\frac{e^{-jk|r-r'|}}{|r-r'|}ds'\right) \\
&\quad -\frac{1}{j\omega\epsilon 4\pi}\sum_{n=1}^{N} I_n \nabla_t \left(\int_{T_n^+} \frac{l_n}{A_n^+}\frac{e^{-jk|r-r'|}}{|r-r'|}ds' - \int_{T_n^-} \frac{l_n}{A_n^-}\frac{e^{-jk|r-r'|}}{|r-r'|}ds'\right) \qquad (2.7)
\end{aligned}$$

2.1.3 Delta-Gap Source Model

Delta-Gap source model is the simplest way which is very suitable to use with RWG edge elements [10]. Delta-gap term refers to an infinitesimally small portion of the antenna, where voltage source is connected, as shown in Figure (2.5).

Delta-Gap voltage source connected to the center of a dipole antenna results in an incident field ,$\overline{E}^i$, at the location of the voltage source on the antenna surface. In our model, delta-gap source corresponds to existence of $\overline{E}^i$ field at only one RWG edge, which is at the source position as shown in Figure 2.5. This approach provides simple implementation for voltage source excitation of antenna and also for antenna input impedance calculation. Input impedance calculation will be defined in the related section.

This delta-gap source implementation results non-zero $\overline{E}^i$ only when observation point is selected at the source point. $\overline{E}^i$ is zero for all observation points selected on the antenna.

If we define $\overline{E}^i$ in the same direction as the surface current flow, as shown in the

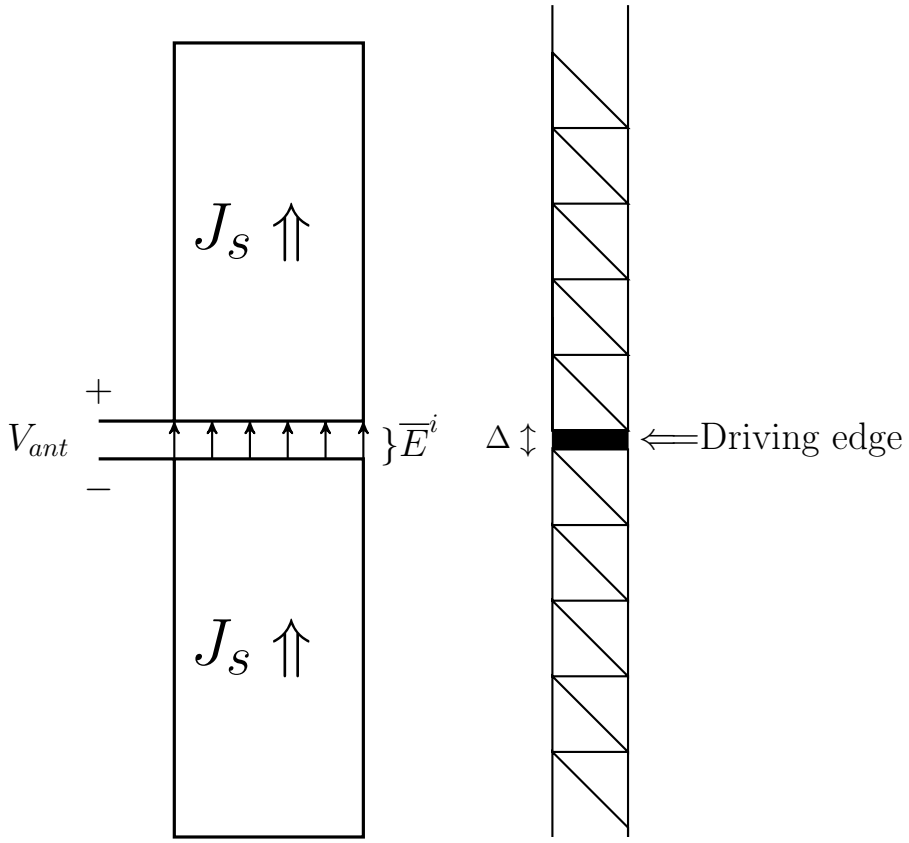

Figure 2.5: Delta-Gap Source Model

Figure 2.5, V_{ant} can be written as:

$$\begin{aligned} V_{ant} &= \int_0^{\Delta} \overline{E}^i \cdot \widehat{a}_z dz \\ &\text{or} \\ \overline{E}^i &= \frac{V_{ant}}{\Delta} \end{aligned}$$

where Δ is the gap width, which tends to zero for Delta-Gap Source model. Then, incident electric field at the feeding edge can be written as:

$$\overline{E}^i = V_{ant}\delta(z)\widehat{a}_z. \tag{2.8}$$

We can now use this result in (2.7).

If the feeding edge is selected as the observation point, since $\overline{E}^i$ defined in (2.8)

is completely tangential (in $\widehat{a_z}$ direction), we can write:

$$V_{ant}\delta(z) = \frac{j\omega\mu}{4\pi}\sum_{n=1}^{N} I_n \int_s \overline{f}_n(r')\frac{e^{-jkR}}{R}ds' - \frac{1}{j\omega\epsilon 4\pi}\sum_{n=1}^{N} I_n \nabla_t \int_s \nabla\cdot\overline{f}_n(r')\frac{e^{-jkR}}{R}ds'$$

$$V_{ant}\delta(z) = \frac{j\omega\mu}{4\pi}\sum_{n=1}^{N} I_n \left(\int_{T_n^+} \frac{l_n}{2A_n^+}\overline{\rho}_n^+(r')\frac{e^{-jk|r-r'|}}{|r-r'|}ds' + \int_{T_n^-} \frac{l_n}{2A_n^-}\overline{\rho}_n^-(r')\frac{e^{-jk|r-r'|}}{|r-r'|}ds'\right)$$

$$-\frac{1}{j\omega\epsilon 4\pi}\sum_{n=1}^{N} I_n \nabla_t \left(\int_{T_n^+} \frac{l_n}{A_n^+}\frac{e^{-jk|r-r'|}}{|r-r'|}ds' - \int_{T_n^-} \frac{l_n}{A_n^-}\frac{e^{-jk|r-r'|}}{|r-r'|}ds'\right). \quad (2.9)$$

At any other observation point on the antenna surface, left hand side, would be zero but right hand side would be the same.

This equation is the discretized form of (2.3) for the dipole antenna geometry studied in this text. The unknowns are current expansion coefficients in this equation. If equation (2.9) is rearranged, it can be seen that, a known voltage source is expressed as the summation of "N" known basis functions $\overline{f}_n$ with "N" unknown coefficients I_n, $(n = 1 \cdots N)$.

$$\overline{V} = I_1\overline{f}_1 + I_2\overline{f}_2 + \cdots + I_N\overline{f}_N$$

To solve this equation which has "N" unknowns, "N" equations are needed. If we write this equation at "N" different observation points (testing points), the "N" necessary equations are obtained. This set of N equations can be solved for the unknown expansion coefficients.

2.1.4 Galerkin Testing Function

Galerkin testing function is used to solve (2.9) in this study. Galerkin Testing Function means testing function $(\overline{f}_m)$ is selected as the same of basis function $(\overline{f}_n)$. Since scattered field $\overline{E}_s$ is known only at the antenna surface, observation points at the equation are selected from there.

We define inner product as

$$\langle\overline{f},\overline{g}\rangle \equiv \int_s \overline{f}\cdot\overline{g}ds.$$

Taking the inner product of both sides of (2.3) with testing function, we get:

$$\begin{aligned} \overline{E}_t^i &= j\omega\overline{A}_t(r) + \nabla_t\Phi(r) \\ \langle\overline{E}_t^i,\overline{f}_m\rangle &= j\omega\langle\overline{A}_t,\overline{f}_m\rangle + \langle\nabla_t\Phi,\overline{f}_m\rangle. \end{aligned}$$

We need to calculate $\langle\overline{A_t},\overline{f}_m\rangle$ and $\langle\nabla_t\Phi,\overline{f}_m\rangle$, where we can use, [17],

$$\langle\nabla_t\Phi,\overline{f}_m\rangle = -\int_t \Phi\nabla_s\cdot\overline{f}_m ds.$$

Since testing functions $(\overline{f}_m)$ are chosen to be same as the expansion functions $(\overline{f}_n)$ and $\nabla\cdot\overline{f}_n$ was calculated in (2.4), it can be shown that:

$$\begin{aligned} \langle\nabla_t\Phi,\overline{f}_m\rangle &= -l_m\left[\frac{1}{A_m^+}\int_{T_m^+}\Phi ds - \frac{1}{A_m^-}\int_{T_m^-}\Phi ds\right] \\ &= l_m\left[\Phi(r_m^{c-}) - \Phi(r_m^{c+})\right] \end{aligned}$$

where $\Phi(r_m^{c\pm})$ are the scalar electric potentials at the center of the plus and minus signed triangles of the testing function. The average of Φ over each triangle is approximated by the value of Φ at the triangle centroid.

With a similar approach, the inner product of the vector magnetic potential $\overline{A}_t$ with testing functions can be written as:

$$\begin{aligned} \langle\overline{A}_t,\overline{f}_m\rangle &= l_m\left[\frac{1}{2A_m^+}\int_{T_m^+}\overline{A}\cdot\overline{\rho}_m^+ ds' + \frac{1}{2A_m^-}\int_{T_m^-}\overline{A}\cdot\overline{\rho}_m^- ds'\right] \\ &= \frac{l_m}{2}\left[\overline{A}(r_m^{c+})\cdot\overline{\rho}_m^{c+} + \overline{A}(r_m^{c-})\cdot\overline{\rho}_m^{c-}\right]. \end{aligned}$$

$\overline{A}(r_m^{c\pm})$ are the vector potentials at the centers of the plus (T_m^+) and minus (T_m^-) signed triangles of the testing element. $\overline{\rho}_m^{c+}$ is the vector defined from free vertex (V_m^+) of the plus signed triangle of the testing element, to the center of that element. $\overline{\rho}_m^{c-}$ is the vector defined from center of the minus signed triangle of the testing element to the free vertex (V_m^-) of the minus signed triangle, as shown in Figure (2.6).

Combining the above results, we get:

$$\langle\overline{E}_t^i,\overline{f}_m\rangle = j\omega\frac{l_m}{2}\left[\overline{A}(r_m^{c+})\cdot\overline{\rho}_m^{c+} + \overline{A}(r_m^{c-})\cdot\overline{\rho}_m^{c-}\right] + l_m\left[\Phi(r_m^{c-}) - \Phi(r_m^{c+})\right] \tag{2.10}$$

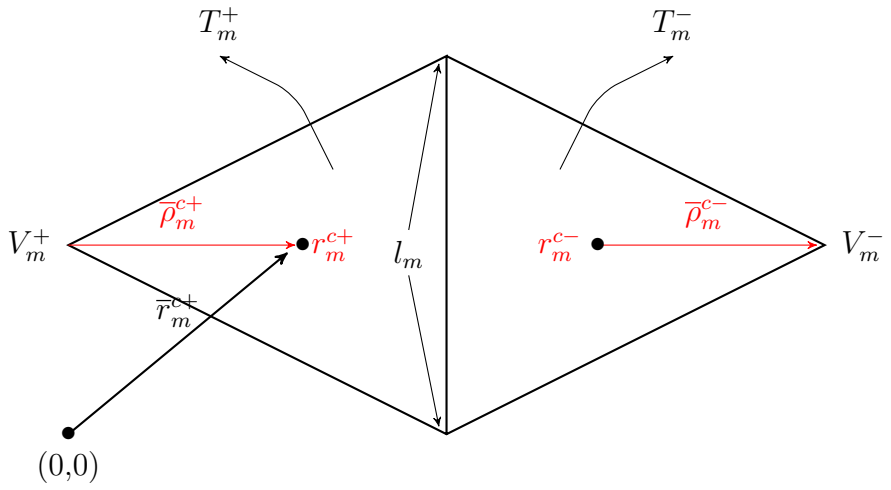

Figure 2.6: Testing RWG Element

We finally use the results derived in the Delta-Gap section in (2.10). If "m" is the index of the feeding edge, by using (2.8) we get

$$\langle \overline{E}_t^i, \overline{f}_m \rangle = \int_{(T_m^+ + T_m^-)} \overline{E}_t^i \cdot \overline{f}_m ds = V_{ant} \int_{(T_m^+ + T_m^-)} \delta(z) \widehat{a_z} \cdot \overline{f}_m ds' = l_m V_{ant}, \quad (2.11)$$

and for all other testing edges on the antenna surface we have

$$\langle \overline{E}_t^i, \overline{f}_m \rangle = 0$$

since $\overline{E}^i$ is zero there, as stated before.

2.1.5 MOM Interaction (Impedance) Matrix

By the use of Galerkin Testing method, we select "N" observation points (as the same of the source points), $m = 1 \cdots N$ to form "N" equations to solve "N" unknown I_n coefficients.

Then, if we combine the results and rewrite (2.10);

$$\begin{aligned} \langle \overline{E}^i, \overline{f}_m \rangle &= j\omega \langle \overline{A}, \overline{f}_m \rangle + \langle \nabla \Phi, \overline{f}_m \rangle \\ &= j\omega l_m \left[\overline{A}(r_m^{c+}) \cdot \frac{\overline{\rho}_m^{c+}}{2} + \overline{A}(r_m^{c-}) \cdot \frac{\overline{\rho}_m^{c-}}{2} \right] + l_m \left[\Phi(r_m^{c-}) - \Phi(r_m^{c+}) \right] \end{aligned}$$

with the following definitions

$$\begin{aligned}
\overline{A}(r_m^{c+}) &= \frac{\mu}{4\pi}\sum_{n=1}^{N} I_n \left[\int_{(T_n^+ + T_n^-)} \overline{f}_n(r')\frac{e^{-jk|\overline{r}_m^{c+}-\overline{r}'|}}{|\overline{r}_m^{c+}-\overline{r}'|}ds'\right] \\
&= \frac{\mu}{4\pi}\sum_{n=1}^{N} I_n \left[\int_{(T_n^+ + T_n^-)} \overline{f}_n(r')\frac{e^{-jk|\overline{r}_m^{c-}-\overline{r}'|}}{|\overline{r}_m^{c-}-\overline{r}'|}ds'\right] \\
\Phi(r_m^{c+}) &= -\frac{1}{j\omega\epsilon 4\pi}\sum_{n=1}^{N} I_n \left[\int_{(T_n^+ + T_n^-)} \nabla\cdot\overline{f}_n(r')\frac{e^{-jk|\overline{r}_m^{c+}-\overline{r}'|}}{|\overline{r}_m^{c+}-\overline{r}'|}ds'\right] \\
&= -\frac{1}{j\omega\epsilon 4\pi}\sum_{n=1}^{N} I_n \left[\int_{(T_n^+ + T_n^-)} \nabla\cdot\overline{f}_n(r')\frac{e^{-jk|\overline{r}_m^{c-}-\overline{r}'|}}{|\overline{r}_m^{c-}-\overline{r}'|}ds'\right]
\end{aligned}$$

where $\overline{r}_m^{c\pm}$ is the vector defined from coordinate center to the center of the plus and minus triangle of the m_{th} testing RWG element, and $\frac{e^{-jk|\overline{r}_m^{c\pm}-\overline{r}'|}}{|\overline{r}_m^{c\pm}-\overline{r}'|}$ is the Green's function.

Then (2.10) becomes:

$$\begin{aligned}
\langle\overline{E}^i,\overline{f}_m\rangle = \sum_{n=1}^{N} I_n \Bigg\{ j\omega l_m \frac{\mu}{4\pi}\Bigg[&\left(\int_{(T_n^+ + T_n^-)} \overline{f}_n(r')\tfrac{e^{-jk|\overline{r}_m^{c+}-\overline{r}'|}}{|\overline{r}_m^{c+}-\overline{r}'|}ds'\right)\cdot\tfrac{\overline{\rho}_m^{c+}}{2} + \\
&\left(\int_{(T_n^+ + T_n^-)} \overline{f}_n(r')\tfrac{e^{-jk|\overline{r}_m^{c-}-\overline{r}'|}}{|\overline{r}_m^{c-}-\overline{r}'|}ds'\right)\cdot\tfrac{\overline{\rho}_m^{c-}}{2}\Bigg] \\
+ l_m \frac{1}{j\omega\epsilon 4\pi}\Bigg[&\left(\int_{(T_n^+ + T_n^-)} \nabla\cdot\overline{f}_n(r')\tfrac{e^{-jk|\overline{r}_m^{c+}-\overline{r}'|}}{|\overline{r}_m^{c+}-\overline{r}'|}ds'\right) - \\
&\left(\int_{(T_n^+ + T_n^-)} \nabla\cdot\overline{f}_n(r')\tfrac{e^{-jk|\overline{r}_m^{c-}-\overline{r}'|}}{|\overline{r}_m^{c-}-\overline{r}'|}ds'\right)\Bigg]\Bigg\}
\end{aligned}$$

and can be replaced by the following system of equations:

$$\langle\overline{E}^i,\overline{f}_m\rangle = \sum_{n=1}^{N} I_n Z_{mn}$$

where $m = 1, \cdots, N$.

The left hand side, namely, $\langle\overline{E}^i,\overline{f}_m\rangle$ is calculated in Section (2.1.4), and we know that:

$$\langle\overline{E}^i,\overline{f}_m\rangle = \begin{cases} l_m V_{ant} & \text{, if m is feeding edge} \\ 0 & \text{, for all other edges} \end{cases} \tag{2.12}$$

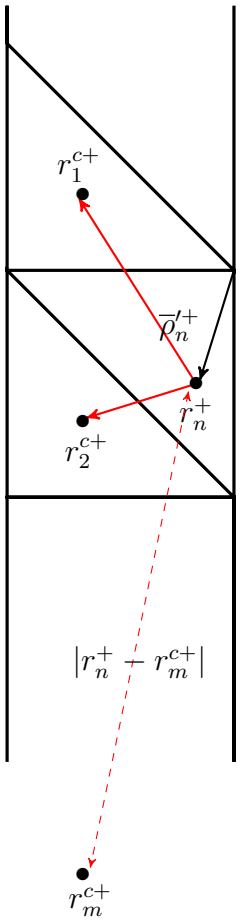

Figure 2.7: Distance between Source and Testing Elements

We can define a vector $\overline{V}$, where $V_m = \langle \overline{E}^i, \overline{f}_m \rangle$ and $m = 1, \cdots, N$:

$$\overline{V} = \begin{bmatrix} V_1 \\ \vdots \\ V_m \\ \vdots \\ V_N \end{bmatrix} = \begin{bmatrix} 0 \\ \vdots \\ l_m V_{ant} \\ \vdots \\ 0 \end{bmatrix}$$

Hence, following equation is obtained:

$$\sum_{n=1}^{N} I_n Z_{mn} = V_m$$

which can be expressed in the matrix form:

$$\begin{bmatrix} Z_{11} & Z_{12} & Z_{13} & \cdots & Z_{1N} \\ Z_{21} & Z_{mn} & & & \vdots \\ \vdots & & \ddots & & \\ Z_{N1} & Z_{N2} & \cdots & & Z_{NN} \end{bmatrix} \begin{bmatrix} I_1 \\ I_n \\ \vdots \\ I_N \end{bmatrix} = \begin{bmatrix} V_1 \\ V_m \\ \vdots \\ V_N \end{bmatrix}$$

We can also express Z_{mn}, named "MoM Interaction (Impedance) Matrix" as:

$$Z_{mn} = l_m \left[j\omega \left(A^+_{mn} \cdot \frac{\rho^{c+}_m}{2} + A^-_{mn} \cdot \frac{\rho^{c-}_m}{2} \right) + \Phi^-_{mn} - \Phi^+_{mn} \right] \tag{2.13}$$

with definitions:

$$A^+_{mn} = \frac{\mu}{4\pi} \left[\int_{T^+_n + T^-_n} f_n(r') \frac{e^{-jk|r^{c+}_m - r'|}}{|r^{c+}_m - r'|} ds' \right]$$

$$A^-_{mn} = \frac{\mu}{4\pi} \left[\int_{T^+_n + T^-_n} f_n(r') \frac{e^{-jk|r^{c-}_m - r'|}}{|r^{c-}_m - r'|} ds' \right]$$

$$\Phi^+_{mn} = -\frac{1}{4j\pi\omega\epsilon} \left[\int_{T^+_n + T^-_n} \nabla \cdot f_n(r') \frac{e^{-jk|r^{c+}_m - r'|}}{|r^{c+}_m - r'|} ds' \right]$$

$$\Phi^-_{mn} = -\frac{1}{4j\pi\omega\epsilon} \left[\int_{T^+_n + T^-_n} \nabla \cdot f_n(r') \frac{e^{-jk|r^{c-}_m - r'|}}{|r^{c-}_m - r'|} ds' \right]$$

As seen from the definitions above, impedance matrix is only dependent on geometry of conductor and the frequency. For the same geometry, impedance matrix should be reevaluated for different frequencies by the use of equation (2.13).

2.1.6 Barycentric Subdivision

Impedance matrix, defined in the equation (2.13) is not completely ready to be calculated numerically. Last step is to introduce a numerical method to calculate the inner integrals of this equation, which are symbolized as $A^{\pm}_{mn}$ and $\Phi^{\pm}_{mn}$.

In these equations integrals are evaluated on the RWG elements that are defined as plus and minus signed triangles. Integrand is either the Green's function,

$G(r') = \frac{e^{-jk|\overline{r}_m^{c\pm} - \overline{r}'|}}{|\overline{r}_m^{c\pm} - \overline{r}'|}$ or its product with $\rho_n^{\pm}(r')$. These integrals can be approximated by replacing the integrand with its value at the centroid of the respective triangle, T_n^+ or T_n^-.

In Section (2.1.4) the testing functions are also approximated with this approach, thus $|\overline{r}_m - \overline{r}'|$ terms in the Green's function are replaced by $|\overline{r}_m^{c\pm} - \overline{r}'|$.

However, there is another point that should be taken into consideration. If this approximation, which was done for testing functions, is applied to basis functions also, Green's function $G(r)$ would be singular at the self-terms (when $m = n$) of the impedance matrix, that is, we would have

$$\frac{e^{-jk|\overline{r}_m^{c\pm} - \overline{r}'|}}{|\overline{r}_m^{c\pm} - \overline{r}'|} = \frac{e^{-jk|\overline{r}_m^{c\pm} - \overline{r}_m^{c\pm}|}}{|\overline{r}_m^{c\pm} - \overline{r}_m^{c\pm}|} = \frac{1}{0}$$

One solution to eliminate this singularity, is to divide the equation into two parts for self-terms and to calculate the singular part analytically while other part is calculated numerically. However, "Barycentric Subdivision Method" is used in this study instead, which corresponds to dividing each triangle into 9 smaller triangles and approximating the integrand by its value at the centers of these smaller triangles, over each sub-triangle.

Hence, integral equation with integrand of Green's function can be calculated as:

$$\begin{aligned} \int_{T_m} G(r')ds' &= \frac{A_m}{9}\sum_{k=1}^{9} G(r'^c_k) \\ \int_{T_m} \frac{e^{-jk|\overline{r}_m^{c\pm} - \overline{r}_n|}}{|\overline{r}_m^{c\pm} - \overline{r}_n|}ds' &= \frac{A_m}{9}\sum_{k=1}^{9} \frac{e^{-jk|\overline{r}_m^{c\pm} - \overline{r}_k^{c}|}}{|\overline{r}_m^{c\pm} - \overline{r}_n|} \end{aligned}$$

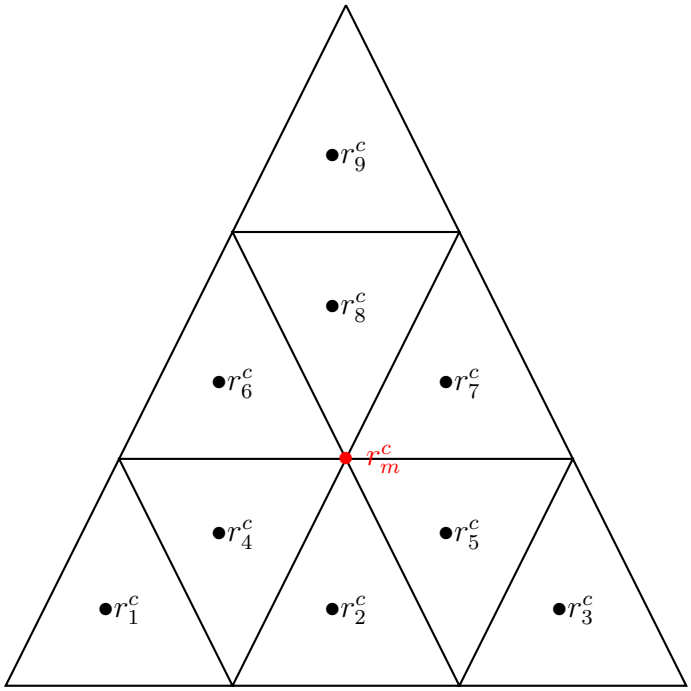

Figure 2.8: Barycentric Subdivision

when it is applied to $A_{mn}^{\pm}$ and $\Phi_{mn}^{\pm}$, we get:

$$
\begin{aligned}
A_{mn}^{\pm} &= \frac{\mu}{4\pi}\left(\int_{T_n^+}\frac{l_n}{2A_n^+}\overline{\rho}_n^+(r')\frac{e^{-jk|r_m^{c\pm}-r'|}}{|r_m^{c\pm}-r'|}ds' + \int_{T_n^-}\frac{l_n}{2A_n^-}\overline{\rho}_n^-(r')\frac{e^{-jk|r_m^{c\pm}-r'|}}{|r_m^{c\pm}-r'|}ds'\right) \\
&= \frac{\mu}{8\pi}\frac{l_n}{9}\left(\sum_{k=1}^{9}\overline{\rho}_n^+(r_k^c)\frac{e^{-jk|r_m^{c\pm}-r_k^c|}}{|r_m^{c\pm}-r_k^c|}ds' + \sum_{k=1}^{9}\overline{\rho}_n^-(r_k^c)\frac{e^{-jk|r_m^{c\pm}-r_k^c|}}{|r_m^{c\pm}-r_k^c|}ds'\right) \\
\Phi_{mn}^{\pm} &= -\frac{1}{4j\pi\omega\epsilon}\left(\int_{T_n^+}\frac{l_n}{A_n^+}\frac{e^{-jk|r_m^{c\pm}-r'|}}{|r_m^{c\pm}-r'|}ds' + \int_{T_n^-}\frac{l_n}{A_n^-}\frac{e^{-jk|r_m^{c\pm}-r'|}}{|r_m^{c\pm}-r'|}ds'\right) \\
&= -\frac{1}{4j\pi\omega\epsilon}\frac{l_n}{9}\left(\sum_{k=1}^{9}\frac{e^{-jk|r_m^{c\pm}-r_k^c|}}{|r_m^{c\pm}-r_k^c|}ds' + \sum_{k=1}^{9}\frac{e^{-jk|r_m^{c\pm}-r_k^c|}}{|r_m^{c\pm}-r_k^c|}ds'\right)
\end{aligned}
$$

By the use of barycentric subdivision, impedance matrix can now be obtained numerically.

2.2 Radiation Parameters

Once surface currents are determined, calculation of radiation fields generated by these currents is straightforward. $\overline{E}$ field can be expressed in terms of vector

and scalar potentials as

$$\overline{E}(r) = -j\omega\overline{A}(r) - \nabla\Phi(r).$$

Using the expansion of surface current in terms of RWG basis functions, we get

$$\begin{aligned}
\overline{A}(r) &= \frac{\mu}{4\pi}\int_s \underbrace{\sum_{n=1}^{N} I_n f_n(r')}_{J(r')}\, G(r,r')ds' \\
\Phi(r) &= -\frac{1}{j\omega\epsilon 4\pi}\int_s \sum_{n=1}^{N} I_n \nabla\cdot f_n(r')G(r,r')ds'
\end{aligned}$$

and the $\overline{E}$ field becomes

$$\overline{E}(r) = \sum_{n=1}^{N} I_n[-\frac{j\omega\mu}{4\pi}\int_s f_n(r')G(r,r')ds' + \frac{1}{j\omega\epsilon 4\pi}\int_s \nabla_t(\nabla\cdot f_n(r'))G(r,r')ds'] \tag{2.14}$$

In the far field region, $\overline{E}$ field can be written by retaining only the terms varying with $1/r$ and eliminating the terms with $1/r^2$ and $1/r^3$, since they become negligible when r is high. Moreover, $\overline{H}$ field can be calculated by the use of

$$\overline{H}(r) = \frac{1}{\eta}\widehat{a_r}\times\overline{E}(r). \tag{2.15}$$

2.2.1 Dipole Model

To calculate both $\overline{E}$ and $\overline{H}$ fields in far and near zones "Dipole Model" can be used as proposed in [9, 10]. In dipole model, an RWG element, consisting of two triangles and a common edge, is replaced by an equivalent small (Hertzian) dipole, from center of the first triangle to the center of the second one. Then, total radiated fields are calculated as sum of fields radiated by all these Hertzian dipoles.

Before replacing the RWG elements with dipoles, equivalent dipole length and current should be found. We will compare the magnetic vector potential $\overline{A}$ of RWG element to that of a Hertzian dipole to find out the equivalent dipole.

Moment of one RWG element is calculated in [17]

$$\overline{m} = \int_{(T_n^+ + T_n^-)} \overline{f}_n(r')ds' = \frac{l_n}{2}(\overline{\rho}_n^{c+} + \overline{\rho}_n^{c-}).$$

Since $\frac{1}{2}(\overline{\rho}_n^{c+} + \overline{\rho}_n^{c-}) = (\overline{r}_n^{c-} - \overline{r}_n^{c+})$ as shown in Figure (2.9), moment becomes

$$\overline{m} \quad = l_n(\overline{r}_n^{c-} - \overline{r}_n^{c+}). \tag{2.16}$$

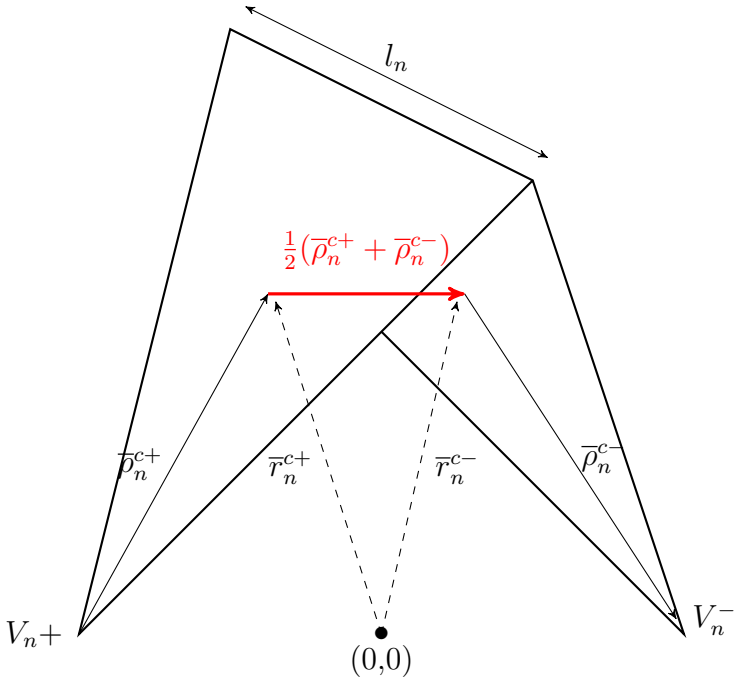

Figure 2.9: Geometry of Vectors

Magnetic potential of an RWG element is given as

$$\overline{A}(r) = I_n[\frac{\mu}{4\pi}\int_{(T_n^+ + T_n^-)} \overline{f}_n(r')\frac{e^{-jk|\overline{r}-\overline{r}'|}}{|\overline{r}-\overline{r}'|}ds'].$$

By the use of (2.16) and approximating the distance between the observation point and the source point $R = |\overline{r} - \overline{r}'|$ by the distance $|\overline{r} - \overline{r}_c|$, where $\overline{r}_c$ is the centroid of the RWG element,

$$\overline{A}(r) = \mu I_n l_n(\overline{r}_n^{c-} - \overline{r}_n^{c+})\frac{e^{-jkR}}{4\pi R}. \tag{2.17}$$

For a Hertzian dipole of length l and current I_0, located at the coordinate origin in $\widehat{a_z}$ direction, generated vector potential $\overline{A}$ is given in [1] as

$$\overline{A}(r) = \mu I_0 l\frac{e^{-jkR}}{4\pi R}\widehat{a_z}$$

where, $R = |\overline{r} - \overline{r}_c|$ and $\overline{r}_c$ is the centroid of the dipole.

If we assume that dipole is positioned in the $(\overline{r}_n^{c-} - \overline{r}_n^{c+})$ direction to be similar with RWG element

$$\overline{A}(r) = \mu I_0 l \frac{e^{-jkR}}{4\pi R} \frac{(\overline{r}_n^{c-} - \overline{r}_n^{c+})}{|\overline{r}_n^{c-} - \overline{r}_n^{c+}|}. \tag{2.18}$$

Equating (2.17) to (2.18) results in

$$\begin{aligned} \mu I_n l_n (\overline{r}_n^{c-} - \overline{r}_n^{c+}) \frac{e^{-jkR}}{4\pi R} &= \mu I_0 l \frac{e^{-jkR}}{4\pi R} \frac{(\overline{r}_n^{c-} - \overline{r}_n^{c+})}{|\overline{r}_n^{c-} - \overline{r}_n^{c+}|} \\ I_n l_n |\overline{r}_n^{c-} - \overline{r}_n^{c+}| &= I_0 l. \end{aligned} \tag{2.19}$$

Here, we may assume $I_0 = I_n l_n$ and $l = |\overline{r}_n^{c-} - \overline{r}_n^{c+}|$. Therefore, an RWG element can be considered to be equivalent to a Hertzian dipole of length $|\overline{r}_n^{c-} - \overline{r}_n^{c+}|$, and current $I_n l_n$.

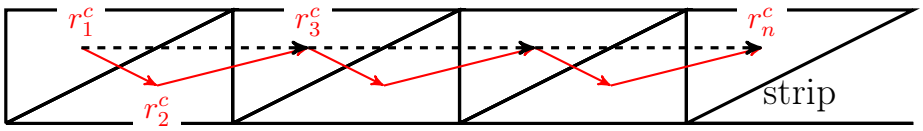

Figure 2.10: Dipole Model

2.2.2 Radiation Fields

By using dipole model, we have "N" Hertzian dipole over the surface of the antenna, since "N" RWG elements are defined.

$\overline{E}$ and $\overline{H}$ fields radiated by the source $\overline{J}$ that is valid for both far and near field regions is, [1]:

$$\overline{E} = -j\frac{1}{4\pi\omega\epsilon} \int_V \left[(\overline{J} \cdot \nabla)\nabla + k^2 \overline{J} \right] \frac{e^{-jkR}}{R} dv' \tag{2.20}$$

$$\overline{H} = -j\frac{1}{4\pi} \int_V \left[\overline{J} \times \nabla \right] \frac{e^{-jkR}}{R} dv' \tag{2.21}$$

These formulas can be used for radiation problem where $\overline{J}_s$ is the induced surface current density and $\overline{E}_s$ and $\overline{H}_s$ are secondary fields created by surface current.

For a single Hertzian dipole, $\overline{J}_s$ turns into $\overline{f}_n I_n$ and R can be taken as r which is the distance from center of the dipole to the observation point.

By reducing the volume integral to surface integral:

$$\overline{E}_n(r) = -j\frac{I_n}{4\pi\omega\epsilon}\int_s \left[k^2\frac{e^{-jkr}}{r}\overline{f}_n + \left(\frac{2}{r^3}+\frac{2jk}{r^2}-\frac{k^2}{r}\right)e^{-jkr}(\overline{f}_n\cdot\widehat{a}_r)\widehat{a}_r\right]ds' \tag{2.22}$$

$$\overline{H}_n(r) = \frac{I_n}{4\pi}\int_s (\overline{f}_n\times\widehat{a}_r)\left[jke^{-jkr}\left(\frac{1}{r}+\frac{1}{jkr^2}\right)\right]ds' \tag{2.23}$$

where $\widehat{a}_r$ is the unit vector in the direction of the observation point.

By the use of (2.16) and (2.19), numerical forms of the equations (2.22) and (2.23) can be written as below [10]:

$$\overline{H}_n(r) = \frac{jk}{4\pi}(\overline{m}\times\overline{r})Ce^{-jkr} \tag{2.24}$$

$$\overline{E}_n(r) = \frac{\eta}{4\pi}((\overline{M}-\overline{m})[\frac{jk}{r}+C]+2\overline{M}C)e^{-jkr} \tag{2.25}$$

where;

$$\begin{aligned}\overline{m} &= I_n l_n(\overline{r}_n^{c-}-\overline{r}_n^{c+})\\ C &= \frac{1}{r^2}[1+\frac{1}{jkr}]\\ \overline{M} &= \frac{(\overline{r}\cdot\overline{m})\overline{r}}{|r|^2}\end{aligned}$$

To calculate the $\overline{E}_n(r)$ field and the $\overline{H}_n(r)$ field due to a single RWG element, (2.24) and (2.25) are used. Total fields at a point r, $\overline{E}_{total}(r)$ and $\overline{H}_{total}(r)$ can be obtained by adding all the fields created by all edge elements.

$$\overline{E}_{total}(r) = \sum_{m=1}^{M}\overline{E}_m(r-\frac{1}{2}(r_m^{c+}+r_m^{c-}))$$

$$\overline{H}_{total}(r) = \sum_{m=1}^{M}\overline{H}_m(r-\frac{1}{2}(r_m^{c+}+r_m^{c-}))$$

2.2.3 Input Impedance, Reflection Coefficient and VSWR

Input impedance is one of the important parameters of the antenna. Calculation of the reflection coefficient Γ, return loss "RL" and the VSWR are straightforward when input impedance is known, since they are directly related.

Antenna input impedance can be defined as the ratio of the feeding voltage strength to the current flowing into the feeding edge. Implementation of Delta-Gap source model with RWG elements provides a simple calculation for the input impedance, since voltage source is thought to be connected to a single RWG element only, as described in Section (2.1.3).

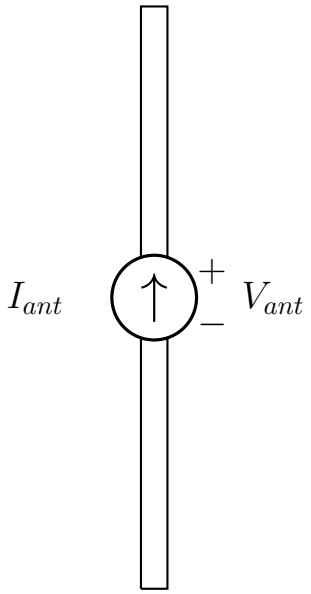

Figure 2.11: Delta-Gap Source Model Simulation

If we excite antenna as shown in Figure 2.11 with voltage source of strength V_{ant}, it will cause a current flow over the feeding RWG edge, which is denoted by I_{ant}. Antenna input impedance can be calculated simply as

$$Z_{in} = \frac{V_{ant}}{I_{ant}} \tag{2.26}$$

As we investigated in Section (3.3.4), all RWG elements can be expressed by an equivalent dipole of length $|\overline{r}_m^{c+} - \overline{r}_m^{c-}|$, and current $(I_m l_m)$. When "m" corresponds to the index of the RWG element at the feed point, we have $V_m = V_{ant} l_m$ in (2.12).

Since I_m coefficients are already calculated and l_m edge lengths and V_m voltage

strength are known, antenna input impedance can easily be calculated.

$$\begin{aligned} V_m &= V_{ant} l_m \\ I_{ant} &= I_m l_m \\ Z_{in} &= \frac{V_{ant}}{I_{ant}} = \frac{V_m}{l_m} \frac{1}{I_m l_m} \\ &= \frac{V_m}{I_m} \frac{1}{(l_m)^2} = \frac{Z_{mm}}{(l_m)^2} \end{aligned}$$

Reflection coefficient (Γ) shows the amount of back reflection of electromagnetic wave which is wanted to be transferred from transmission line to the antenna. It is the result of the mismatch of the antenna input impedance and the characteristic impedance of the transmission line. It is defined as;

$$\Gamma = \frac{Z_{in} - Z_0}{Z_{in} + Z_0}$$

where Z_0 is the characteristic impedance of the transmission line that connects the source to the antenna. VSWR is defined as;

$$VSWR = \frac{1 + |\Gamma|}{1 - |\Gamma|}$$

In all applications, reflection coefficient (Γ) and VSWR are desired to be low. Matching networks are used to decrease the back reflection at the input antenna port in the following sections.

2.2.4 Radiation Density, Radiated Power, Directivity and Gain

2.2.4.1 Radiation Density

Radiation density, (W) is defined as average power of the radiated field per unit area and it is calculated by the "Poynting Vector" [1].

$$\overline{W}(r) = \frac{1}{2} Re[\overline{E}(r) \times \overline{H}^*(r)] \tag{2.27}$$

Once $\overline{E}$ and $\overline{H}$ fields are determined by the use of formulas (2.25) and (2.24), radiated power at any observation point can be calculated by (2.27).

In the far field, $\overline{E}$ and $\overline{H}$ fields and the propagation vector are mutually orthogonal. This means that the radiation density (W) is in the propagation direction in the far field region.

$$\overline{W}(r) = \frac{1}{2\eta}|\overline{E}(r)|^2\widehat{a}_r$$

2.2.4.2 Total Radiated Power

To find out the total radiated power P_{rad}, we should integrate Poynting vector over a closed surface surrounding the transmitter antenna.

$$P_{rad} = \int_s \frac{1}{2\eta}|\overline{E}(r)|^2 ds'$$

"s" is the surface surrounding the antenna.

2.2.4.3 Radiation Resistance

Once the total radiated power P_{rad} is calculated, we can calculate the radiation resistance. If antenna is thought as a radiator, following formula can be written to calculate the radiated power [1]:

$$P_{rad} = \frac{1}{2}R_{rad}|I|^2.$$

Then radiation resistance can be calculated as:

$$R_{rad} = \frac{2P_{rad}}{|I|^2}$$

where I is the feed current.

2.2.4.4 Feed Power

Feed power is the power input to the antenna at the feeding edge. This is the input power that will be radiated.

$$P_{feed} = \frac{1}{2}Re(IV^*) = \frac{1}{2}Re(Z_{in}|I|^2)$$

V is the source voltage at the feed and I is the feed current. Z_{in} is the input impedance calculated in Section 2.2.3 and real part of the input impedance is equal to the radiation resistance R_{rad} an for ideal antenna. So, for lossless ideal antenna, "Feed Power" (P_{feed}) and the "Total Radiated Power" (P_{rad}) are equal. It means that, antenna radiates all the power fed to the antenna.

2.2.4.5 Directivity

Directivity is another parameter that is used for analyzing antennas. Directivity function is defined as the ratio of the power radiated by the antenna in a given direction to the power that would be radiated in the same direction if all the radiated power were distributed uniformly to the space. Directivity is given by the following formula:

$$Directivity = \frac{W(\theta,\phi)(4\pi r^2)}{P_{rad}^{total}}.$$

2.2.4.6 Antenna Efficiency

Efficiency of an antenna (e_0) can be defined by considering two type of losses; losses due to the reflections at the antenna terminal because of the mismatch (e_r) and losses due to the structure of the antenna (e_{cd}). In general efficiency can be calculated as:

$$e_0 = e_r e_{cd}$$

where $e_r = 1 - |\Gamma|^2$ and e_{cd}=conduction and dielectric efficiency. e_{cd} is also named as antenna radiation efficiency [1].

2.2.4.7 Gain

Antenna gain represents, the ratio of the power radiated in a given direction to the power that would be radiated in the same direction if all the power were distributed uniformly to space. Directivity and gain are similar parameters but, former is calculated using the radiated power, while the latter is calculated using the input power. For an ideal antenna, directivity and gain are identical since all the input power would be radiated. However, since there are always losses in real life, gain and directivity are related by the antenna radiation efficiency.

$$Gain = \frac{W(\theta, \phi)(4\pi r^2)}{P_{in}}$$

$$Gain = e_{cd} Directivity$$

2.2.4.8 Absolute Gain

In the gain definition, losses due to the mismatch between the transmission line and the antenna (e_r) are not taken into account. Thus we can introduce a definition, absolute gain, that considers also the reflection loss [1]

$$\begin{aligned} G_{abs} &= e_r Gain = (1 - |\Gamma|^2) Gain \\ &= e_0 Directivity. \end{aligned} \tag{2.28}$$

Absolute gain is proportional to the ratio of power delivered to the observation point to the power that is generated from voltage source of the antenna. For this reason absolute gain is named also as "system gain". [19]

CHAPTER 3

LOADED DIPOLE ANTENNA ANALYSIS

3.1 Antenna Loading

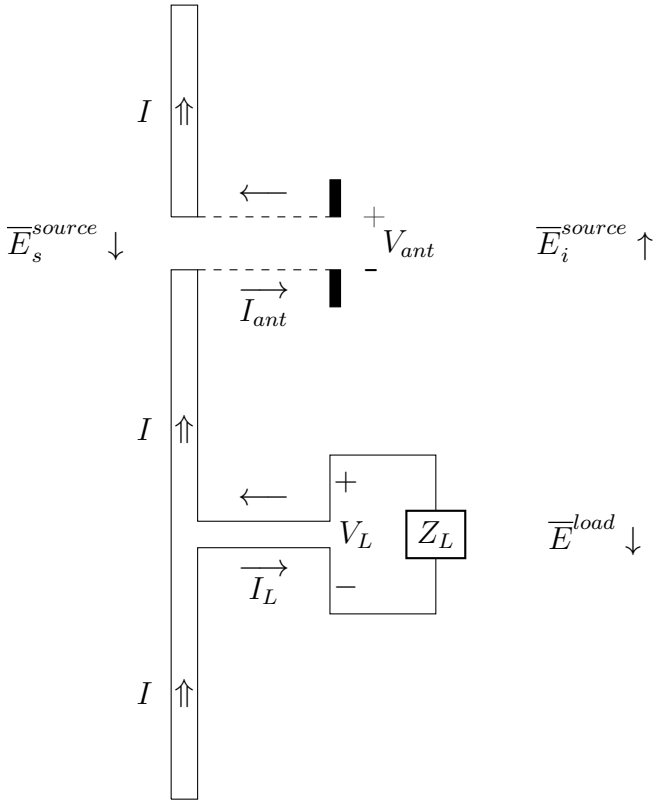

Figure 3.1: Geometry of Loaded Dipole

To formulate the problem with lumped loads, we will reconsider the derivation. The scattered field is given as

$$\overline{E}_s = -j\omega\overline{A} - \nabla\Phi$$

where the scattered field $\overline{E}_s$ is related to the incident field $\overline{E}_i$ by the use of boundary condition; $\overline{E}_t^{total}$ should vanish over the surface of the antenna.

The standard MoM formulation yields

$$\langle \overline{E}^i, \overline{f}_m \rangle = \sum_{n=1}^{N} I_n Z_{mn}.$$

On the antenna surface this equation can be expressed as

$$\langle -\overline{E}^s, \overline{f}_m \rangle = \sum_{n=1}^{N} I_n Z_{mn} \tag{3.1}$$

where we have

$$\langle \overline{E}^i, \overline{f}_m \rangle = \langle -\overline{E}^s, \overline{f}_m \rangle = l_m V_{ant}$$

if m is the feeding edge. For all edges except the feeding edge

$$\langle \overline{E}^i, \overline{f}_m \rangle = \langle -\overline{E}^s, \overline{f}_m \rangle = 0$$

since $\overline{E}^i$ exists only at the feeding edge.

The method used for inserting a lumped load to the antenna is similar to what we have done for Delta-Gap voltage source excitation. Load is assumed to be connected to a single RWG element as shown in Figure 3.2.

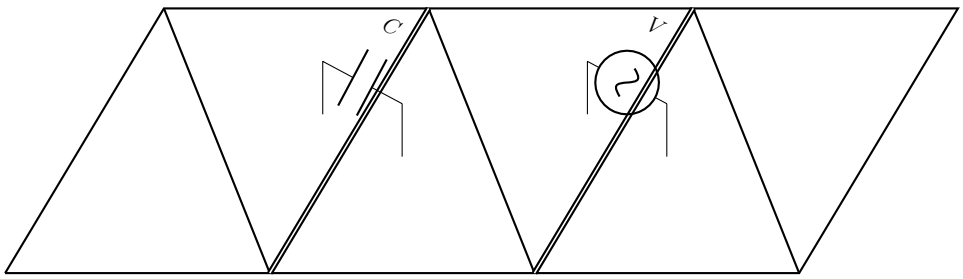

Figure 3.2: Loading of Voltage Source and Lumped Load

The presence of, loading causes a modification of boundary condition at the loaded edge. The tangential component of the total electric field is no longer zero at the load position but it is equal to $\overline{E}^{load}$ [12, 13].

$$\overline{E}^{total} = \overline{E}^i + \overline{E}^s = \overline{E}^{load} = -\frac{V_L}{d}$$

where d is the gap width of the port that load is connected. As d tends to zero

$$\overline{E}^{load} = \overline{E}^{i} + \overline{E}^{s} = -V_L \delta(z - z_k)$$

where z_k is the load position. Since $\overline{E}^{i} = 0$ at the loaded edge k

$$\overline{E}^{s} = -V_L \delta(z - z_k). \tag{3.2}$$

Equation (3.2) is in the form of (2.8). Then by the use of (2.11), we get

$$\langle -\overline{E}^{s}, \overline{f}_k \rangle = V_L l_k$$

where $\overline{f}_k$ is the testing function at the loaded edge k and l_k is the length of the loaded edge k.

Then by the use of (3.1)

$$\langle -\overline{E}^{s}, \overline{f}_k \rangle = \sum_{n=1}^{N} I_n Z_{kn} = V_L l_k$$

$$Z_{k1} I_1 + Z_{k2} I_2 + \ldots + Z_{kk} I_k + \ldots + Z_{kN} I_N = V_L l_k$$

The terminal equation of the load $V_L = -I_L Z_L$ must be satisfied at the load, where I_L is the current flowing over the loaded edge, $I_L = I_k l_k$ (2.19)

$$Z_{k1} I_1 + Z_{k2} I_2 + \ldots + Z_{kk} I_k + \ldots + Z_{kn} I_N = -I_k Z_L {l_k}^2$$

Rearranging this equation, we get

$$Z_{k1} I_1 + Z_{k2} I_2 + \ldots + (Z_{kk} + Z_L {l_k}^2) I_k + \ldots + Z_{kn} I_N = 0$$

and the MoM matrix equation becomes

$$\begin{bmatrix} Z_{11} & Z_{12} & Z_{13} & \cdots & Z_{1n} \\ Z_{21} & \ddots & & & \vdots \\ \vdots & & (Z_{kk} + Z_L {l_k}^2) & & \\ Z_{m1} & Z_{m2} & \cdots & & Z_{mn} \end{bmatrix} \begin{bmatrix} I_1 \\ \vdots \\ I_k \\ I_n \end{bmatrix} = \begin{bmatrix} V_1 \\ \vdots \\ V_k \\ V_m \end{bmatrix}$$

This result shows that the antenna loading can be taken into account by a modification of the loaded self-term elements of the MoM Impedance matrix. This method provides great convenience, especially in computer programming.

Since loading effects only the self-terms of the MoM matrix, loaded antenna impedance matrix can be written as the sum of two matrices

$$[Z][I] = ([Z^0] + [Z^L])[I] = [V] \tag{3.3}$$

where $[Z^0]$ is the NxN impedance matrix without loading and $[Z^L]$ is the loaded impedance matrix with diagonal elements $Z_L {l_k}^2$. Only the loaded edge (k) self-terms (Z_{kk}) of $[Z_L]$ are nonzero [14]. If load values are changed, there is no need to calculate Z^0 again, since it doesn't contain loading effects, only $[Z^L]$ is to be modified for different load values. Since load number (k) is usually very small compared to the edge number (N), this method provides simplicity especially in load value optimization process. Details will be given in the corresponding section.

3.2 Matching Network

As discussed in Section (2.2.3), VSWR and the reflection coefficient (Γ) are very important parameters for antenna designers. Especially for broadband dipole antenna designs, providing small VSWR and small reflection coefficient are mostly one of the hardest subjects of optimization since dipole antennas have VSWR peaks at frequencies for which dipole length is an integer multiple of wavelength (λ). To decrease the VSWR, a matching network can be connected to the input of the antenna. The task of the matching network is to provide stable and appropriate input impedance over the operational frequency range of the antenna.

Matching network, used in this study consist of a parallel inductance and a transformer. Figure 3.3 shows the matching network. Z_A is the antenna input impedance defined in Section (2.2.3). By the use of matching network, input

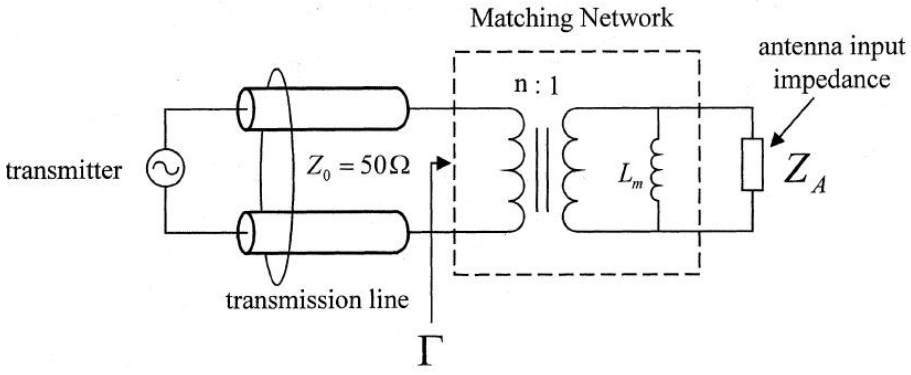

Figure 3.3: Matching Network

impedance Z_{in} is calculated as;

$$Z_{in} = n^2(Z_{L_m}//Z_A) \tag{3.4}$$

where, "n" is the transformer turns ratio, and Z_{L_m} is the impedance of the inductance used in matching network, $Z_{L_m} = j\omega L_m$.
Since characteristic impedance (Z_0) of the transmission line is taken as 50 Γ, we get

$$\Gamma = \frac{Z_{in} - 50}{Z_{in} + 50}$$

$$VSWR = \frac{1 + |\Gamma|}{1 - |\Gamma|}$$

where "n" and the Z_{L_m} are the parameters, that can be optimized to have lower Γ and VSWR.

3.3 Validation of the Code

In this section, antenna analysis code that is developed in MATLAB is investigated. This code is based on the procedure described up to this point. Strip antenna surface is divided into planar triangular grids and RWG basis function is defined on these triangles. By the use of (2.13), MoM impedance matrix is obtained and surface currents are calculated. Numerical formulas (2.25) and

(2.24) are then used to calculate the radiation fields created by these surface currents.

For loaded dipole antenna analysis, impedance matrix is modified based on the load positions and values. After then, the same procedure is used to calculate the radiation fields. To investigate the broadband behavior of the unloaded and loaded dipole antennas, calculations are done over a selected broad frequency band and results are demonstrated as a function of frequency. Verification of the developed code is done by comparing the results with the NEC.

3.3.1 Mesh Generation

Antenna surface is divided into planar triangular patches since RWG basis function is defined on triangular grids. When the length and the width of the strip antenna is determined, triangular mesh modeling can be easily performed. Formulation in [20] is used to generate automatic triangular mesh over the strip surface. This formulation is applicable to all rectangular objects.

Since the width of the dipole antenna is very small compared to its length, surface current has only axial component ($\widehat{a}_z$) according to the thin wire theory [14]. Therefore, width of the strip is covered by only two triangles to form a single RWG element in this direction, whereas length of the strip is divided into numerous triangles to handle the current distribution in this direction. As the triangle patch dimensions are decreased, the results approximate better to the real results, since smaller mesh dimensions correspond to more samples over the computational domain.

In the developed program, coordinate information of the mesh is saved in two variables:

$t(3 \times N)$ - Node number for each triangle. One column represents three nodes

of a single triangle. Total number of triangles is N.

$$t = \begin{bmatrix} 1 & 2 & \dots \\ 2 & 4 & \dots \\ 3 & 3 & \dots \end{bmatrix}$$

$p(3 \times P)$ - Cartesian Node Coordinates, one column represents position of a single node in x, y and z coordinates. Total number of nodes is P.

$$p = \begin{bmatrix} 0 & 5 & 5 & 10 & \dots \\ 2.5 & 0 & 5 & 2.5 & \dots \\ 0 & 0 & 0 & 0 & \dots \end{bmatrix}$$

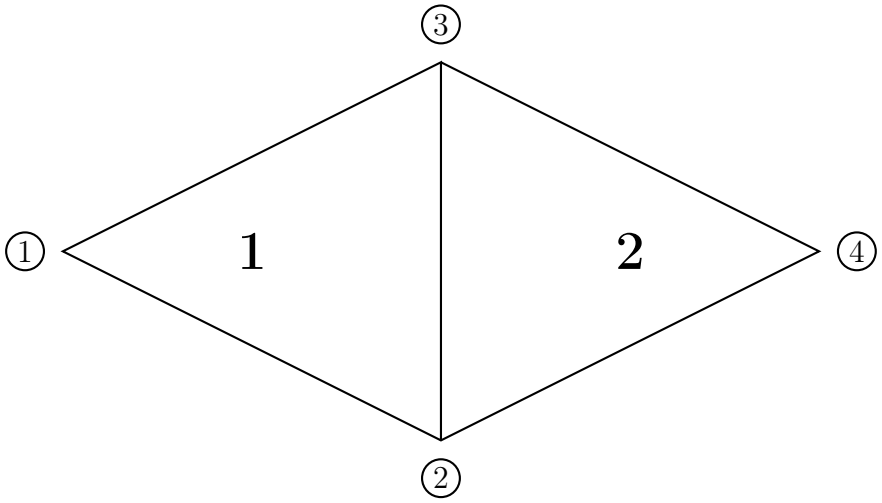

Figure 3.4: Mesh Geometry

3.3.2 Frequency Sweep

Frequency dependence of the impedance matrix is investigated in the Section (2.1.5). For broadband antennas, analysis should be done over desired broad frequency band. Therefore, frequency should be swept over the frequency range in "N" steps which results in repeating the calculation of the impedance matrix "N" times.

Frequency step number should be selected high enough to take more samples over the frequency range. Although, high sampling rate increases the process-

ing work, since some parameters may change dramatically with the changing frequency (such as gain), dense sampling is needed [2].

3.3.3 Numerical Electromagnetic Code (NEC)

To validate the code developed in MATLAB, NEC results are used as reference. NEC is an antenna simulation program that gives enough approximate values for the basic antenna parameters; forward gain, input impedance, reflection coefficient and VSWR. These four parameters are selected as the criterion to compare our results to the NEC results.

Basic difference between NEC and our analysis is the antenna construction method. NEC simulates 3D, circular wire antennas. However, we modeled the dipole antenna as a rectangular strip [3]. An equivalent strip width is given as $a = 0.25a_{eqv}$ in [10], where "a" is the radius of the dipole and "a_{eqv}" is the width of the strip. This equivalence is examined by comparing the results. For this purpose, examples are repeated for strip models with different widths and different grid dimensions.

3.3.4 Dipole Antenna without Loading

As a first example we consider an unloaded, center fed dipole antenna of length 30 cm. In NEC, the radius is taken as 0.125 cm and the surface of the antenna is divided into 61 equal segments. For comparison purposes, the radius (a) and the segment number of the NEC model is kept constant.

Forward gain is defined in terms of spherical coordinates of θ and ϕ in NEC. Since dipole antenna has symmetric radiation pattern in azimuth, ϕ can be chosen arbitrarily. Whereas, θ is taken as 90 degrees for forward gain. In our model, antenna is positioned in x-z plane, and observation point is selected across the feeding edge, i.e. x=0 cm, z=15 cm and y arbitrary.

Several dipole antennas are considered with different strip widths to find the equivalent strip antenna for cylindrical dipole with radius of 0.125 cm. Figures

3.6, 3.7 and 3.8, show the results for strip widths of 0.125cm, 0.375 cm and 0.5 cm, respectively. According to the results, strip width of 0.375 cm and 0.5 cm with 120 triangles gave very close results to NEC. Therefore, for dipole of radius 0.125 cm, strip of width 0.375 cm ($a = 0.3a_{eqv}$) and 0.5 cm ($a = 0.25a_{eqv}$) can be taken as an equivalent strip antenna, verifying the statements in [10, 22]. An additional case is also considered to show the effect of grid number in Figure(3.9). If we compare the two strip models of width 0.5 cm with different triangle numbers, shown in Figures (3.8) and (3.9), strip model with 120 triangles gave better results than the model with 60 triangles. This is an expected result, since dipole antenna in NEC is modeled as 61 equal cylindrical segments, which can be thought as combination of two adjacent triangle patches of our strip model.

For unloaded dipole, it can be seen from the "Input Reactance" graphs that, first resonance occurs when $l = \lambda/2$ (actually $0.47 - 0.48\lambda$), which corresponds to 470-480 MHz and repeats in every $\lambda/2$ steps in frequency. Moreover, from the "Input Resistance" graphs it is seen that, at the frequencies where $l = \lambda$ and multiples, input resistance becomes high, because of the very low current at the feed point. Conversely, current at the feed point is high when $l = \lambda/2$ and odd multiples, resulting in low input resistance. Since input resistance is close to 50 Ω at the first resonance point (almost 70 Ω), reflection coefficient is very low. When $l = \lambda$, (actually $0.8-0.9\lambda$) second resonance (anti-resonance) occurs. At this point, reflection coefficient is high because of the high input resistance (larger than 1000 Ω).

Operating frequency band of a dipole antenna is typically limited with the low reflection coefficient regions. Broadband optimization applications attempts to decrease the reflection coefficient over much wider frequency bands.

According to [4], as the antenna radius is increased, the reactance and the resistance of the antenna become more nearly uniform, resulting in broader band. Moreover, resonance frequencies also get smaller as the antenna becomes thicker.

3.3.5 Loaded Dipole Antenna

To investigate the effects of the resistive, capacitive and inductive loading, they are considered separately. Graphs are drawn only for the equivalent strip antenna of 0.5 cm width with 120 triangles.

For resistive loading, Figures (3.10) and (3.11); for capacitive loading, Figures (3.12) and (3.13); for inductive loading, Figures (3.14) and (3.15) are given below as examples. In all cases, there are two equal loads located at $l/4$ and $3l/4$, where l is the antenna length. Only the load values are changed. The same geometries are also solved in NEC and results are included in respective figures.

According to the results, resistively loaded dipoles, represent smoother impedance and gain behavior compared to unloaded dipole. Average VSWR is decreased and minimum gain is increased over the bandwidth with resistive loading. Capacitive loading also results in smoother impedance behavior. Moreover it causes impedance curves to shift slightly to right (higher resonance frequencies). Therefore, resonance frequency increases and antenna behaves as if it were shorter than it really is [10]. The effect of capacitive loading is more prominent when the load capacitance is smaller as can be seen from a comparison of Figures (3.12) and (3.13). On the other hand, inductive loading causes dipole to behave as if it were longer then it physically is, i.e., shifts the curves to the left.

3.3.6 Dual-band Dipole Antenna

Parallel-tuned resonant circuits can be used with a long dipole to constitute a multi-band dipole antenna that operates as a shorter dipole at high frequency and as a longer dipole at lower frequency. For the structure shown in Figure (3.5), the L-C circuit is chosen to be resonant at the frequency where l_1 becomes half-wavelength ($l_1 = \lambda/2$). The resonant circuit provides a very high impedance and isolates the outer portions of the dipole from the inner section at this frequency. At some desired lower frequency the L-C circuit has a net inductive reactance and forms a loading coil to tune the dipole antenna of length l[4]. This is known as antenna trap.

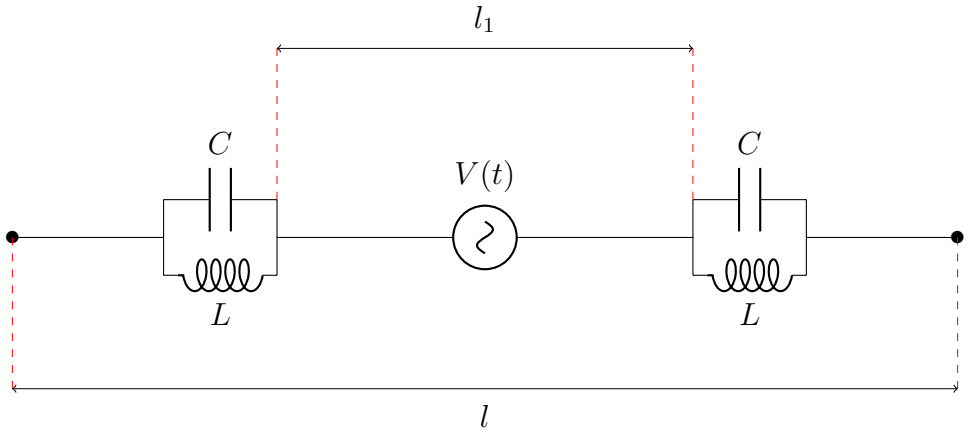

Figure 3.5: L-C Trap Antenna

To implement a trap, 2 parallel L-C circuits are included in a 30 cm dipole at positions $l/4$ (7.5 cm) and $3l/4$ (22.5 cm). Therefore, the distance between traps is l_1=15 cm. At the frequency where l_1 becomes half-wavelength, L-C trap should resonate and isolate the outer parts. Since l_1=15 cm, the desired resonance frequency can be calculated as 1 GHz. Therefore, the L-C trap should resonate at 1 GHz.

$$\begin{aligned} \omega &= \frac{1}{\sqrt{LC}} = 2\pi f = 2\pi 10^9 \\ \sqrt{LC} &= \frac{1}{2\pi 10^9} \\ LC &= \frac{1}{4\pi^2} 10^{-18} = 25 \times 10^{-21} \end{aligned} \tag{3.5}$$

At the lower frequency of 500 MHz, where full length (l =30 cm) of the antenna becomes half-wavelength, L-C circuit doesn't resonate and has a net reactance which is proportional to the inductance value of L. Therefore, antenna behaves like a inductively loaded dipole at this frequency.

To decrease the load effect and the loss, L can be selected low, i.e., L=5nH. Moreover, C should be chosen to satisfy the equation (3.5), i.e., C=5pF. Therefore, we expect antenna to resonate at 1 GHz because of the trap and at 500 MHz and the odd multiple frequencies, because of the 30 cm length inductively loaded dipole. The results are shown in Figure (3.16) and are in agreement with the above discussion.

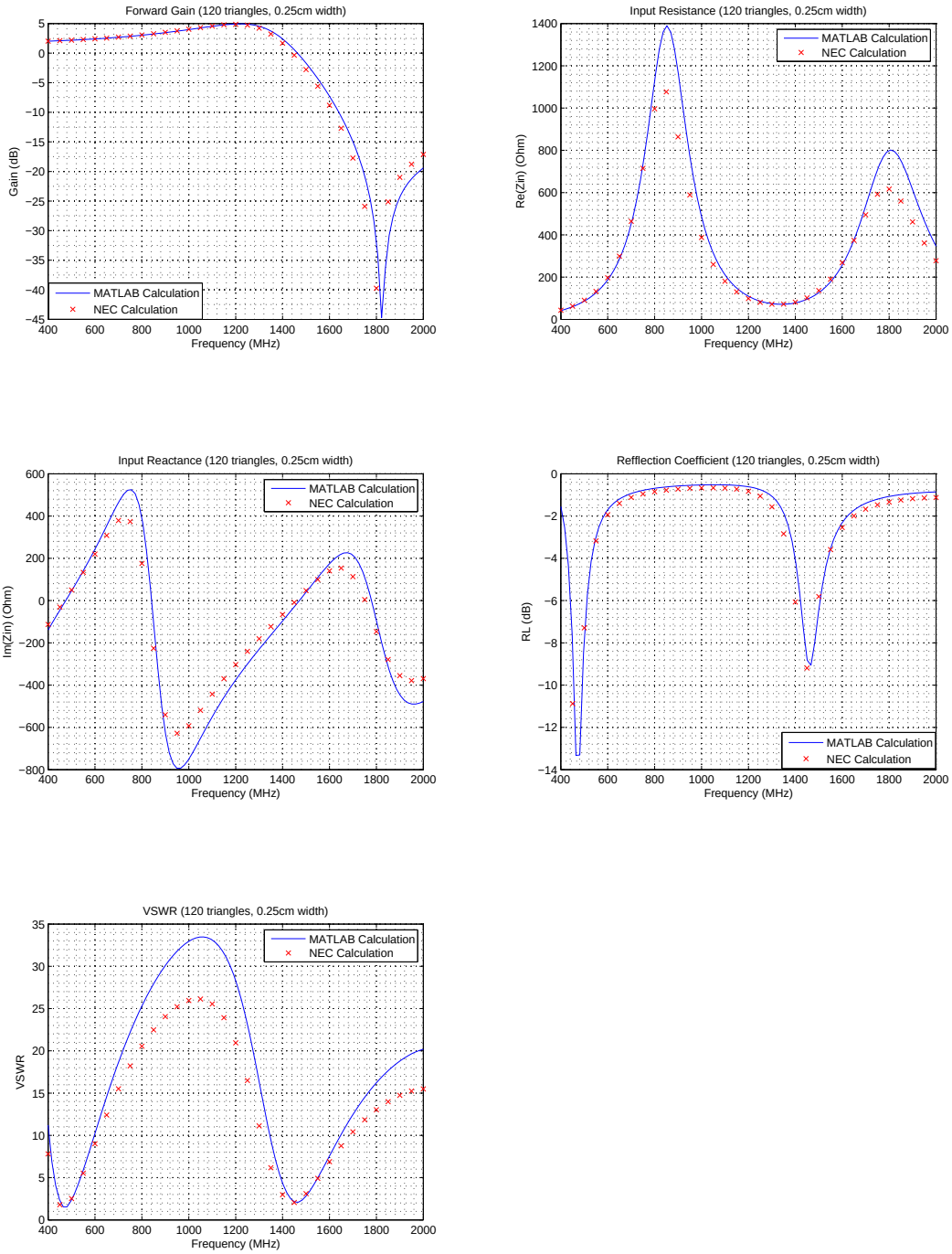

Figure 3.6: Unloaded Dipole Antenna; l=30 cm, w=0.25 cm with 120 triangles

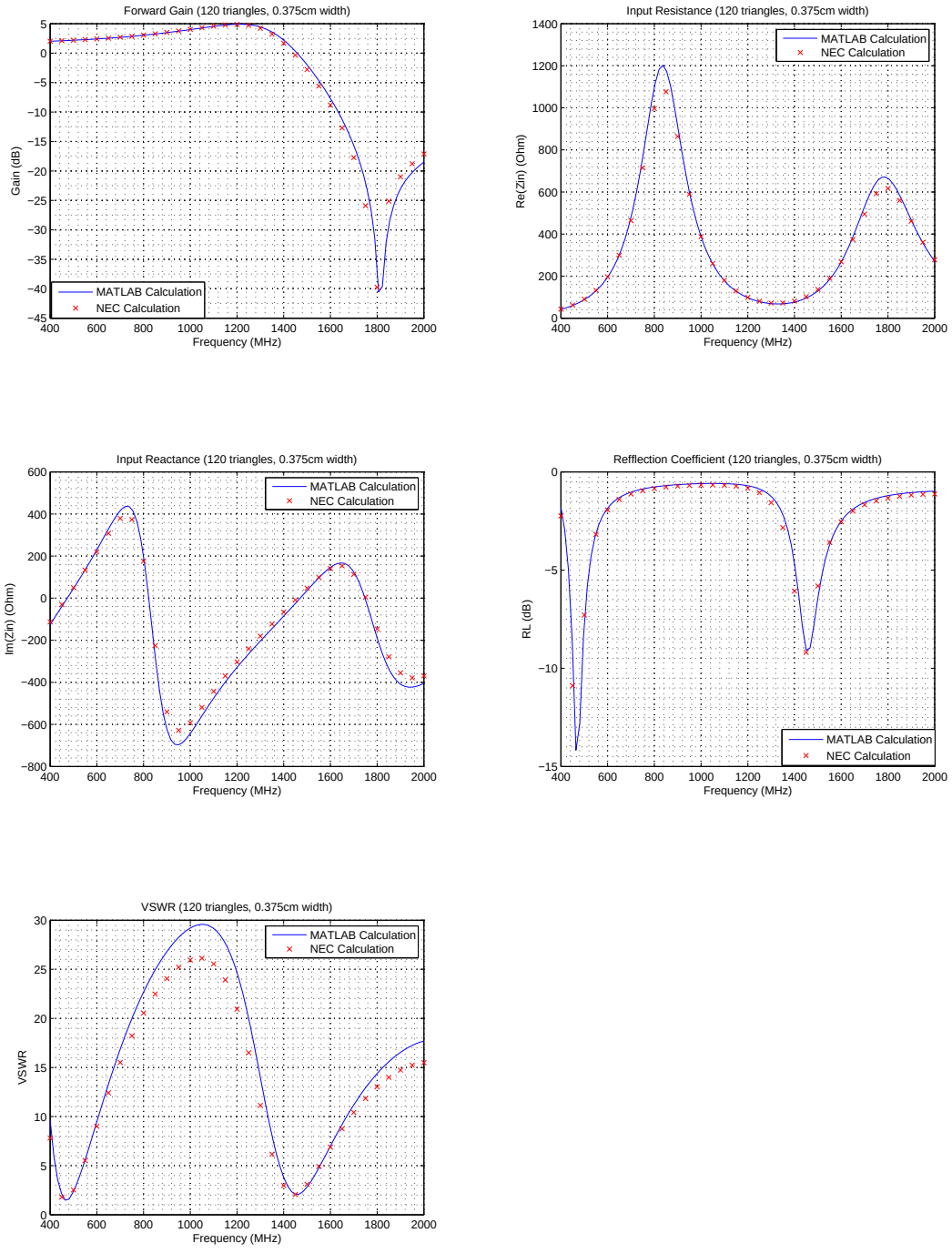

Figure 3.7: Unloaded Dipole Antenna; l=30 cm, w=0.375 cm with 120 triangles

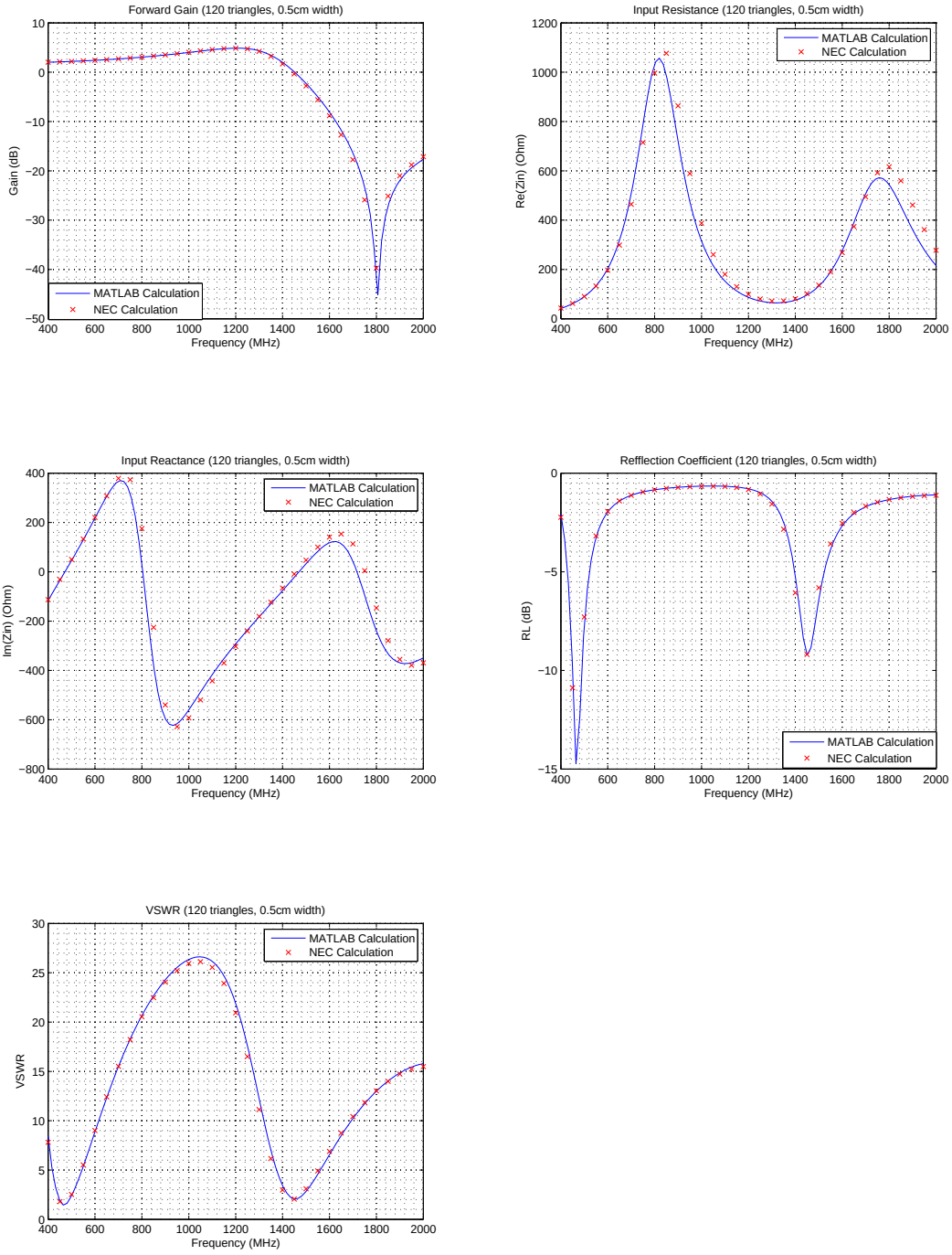

Figure 3.8: Unloaded Dipole Antenna; l=30 cm, w=0.5 cm with 120 triangles

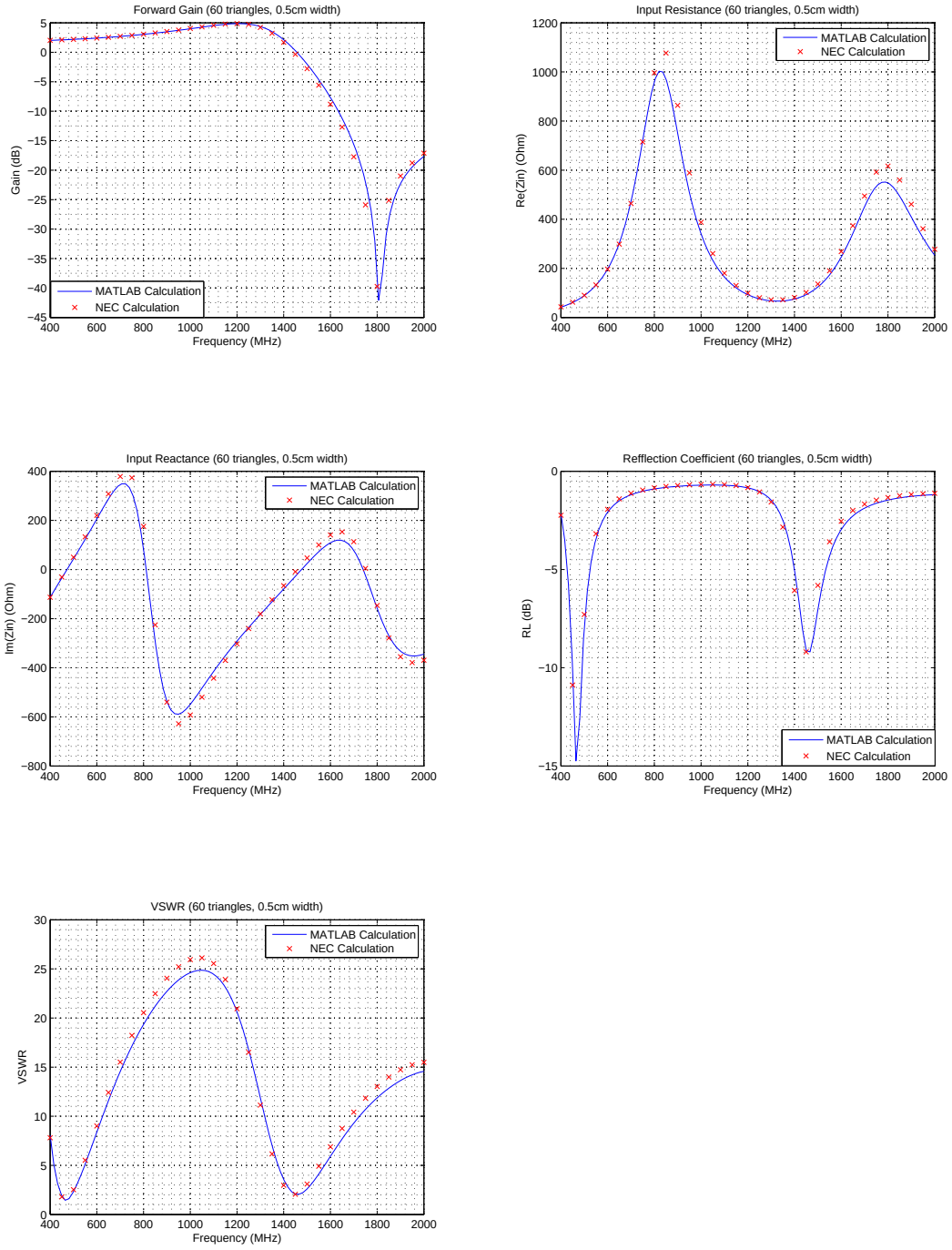

Figure 3.9: Unloaded Dipole Antenna; l=30 cm, w=0.5 cm with 60 triangles

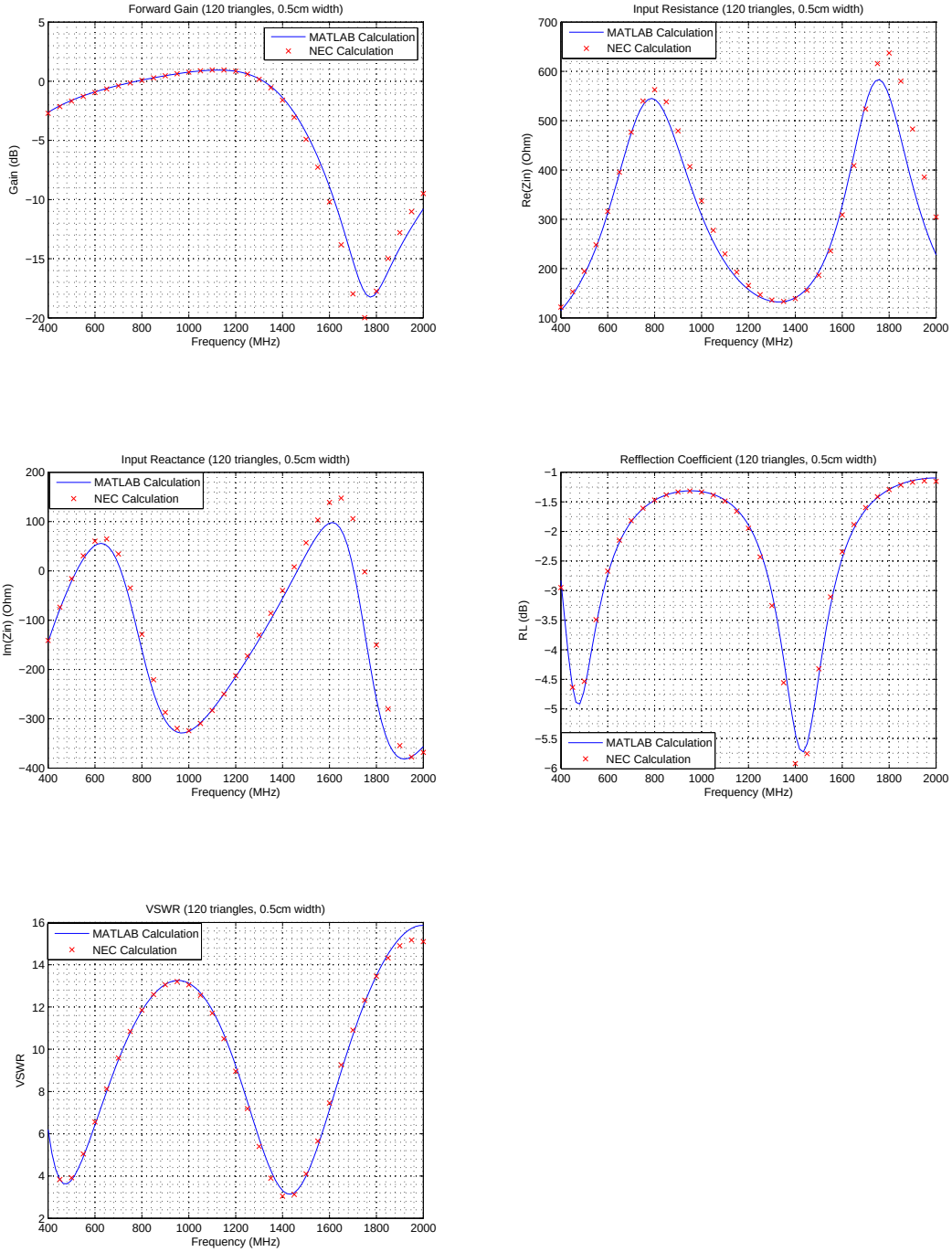

Figure 3.10: Resistively Loaded Dipole Antenna; 2x100 Ω at $l/4$ and $3l/4$

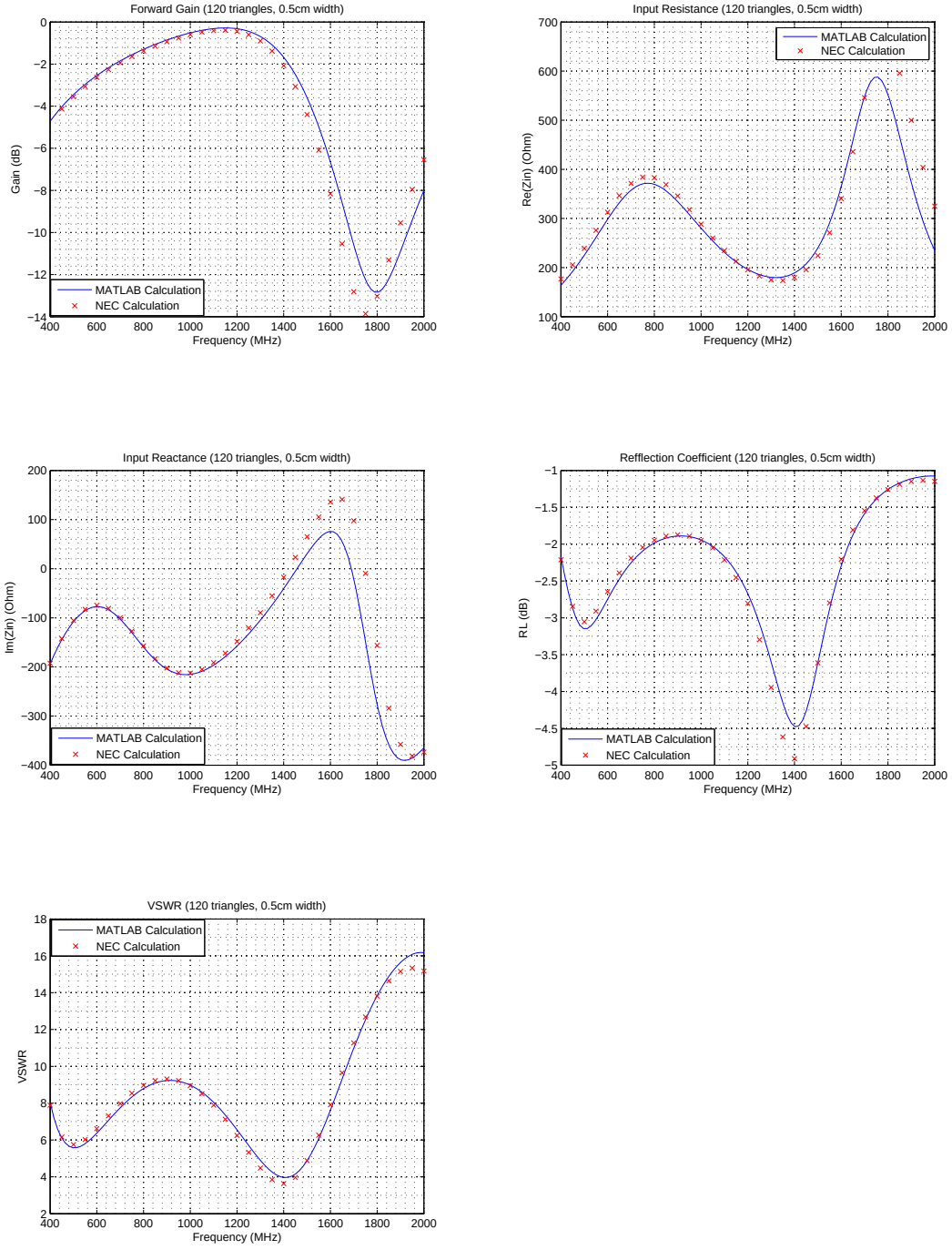

Figure 3.11: Resistively Loaded Dipole Antenna; 2x200 Ω at $l/4$ and $3l/4$

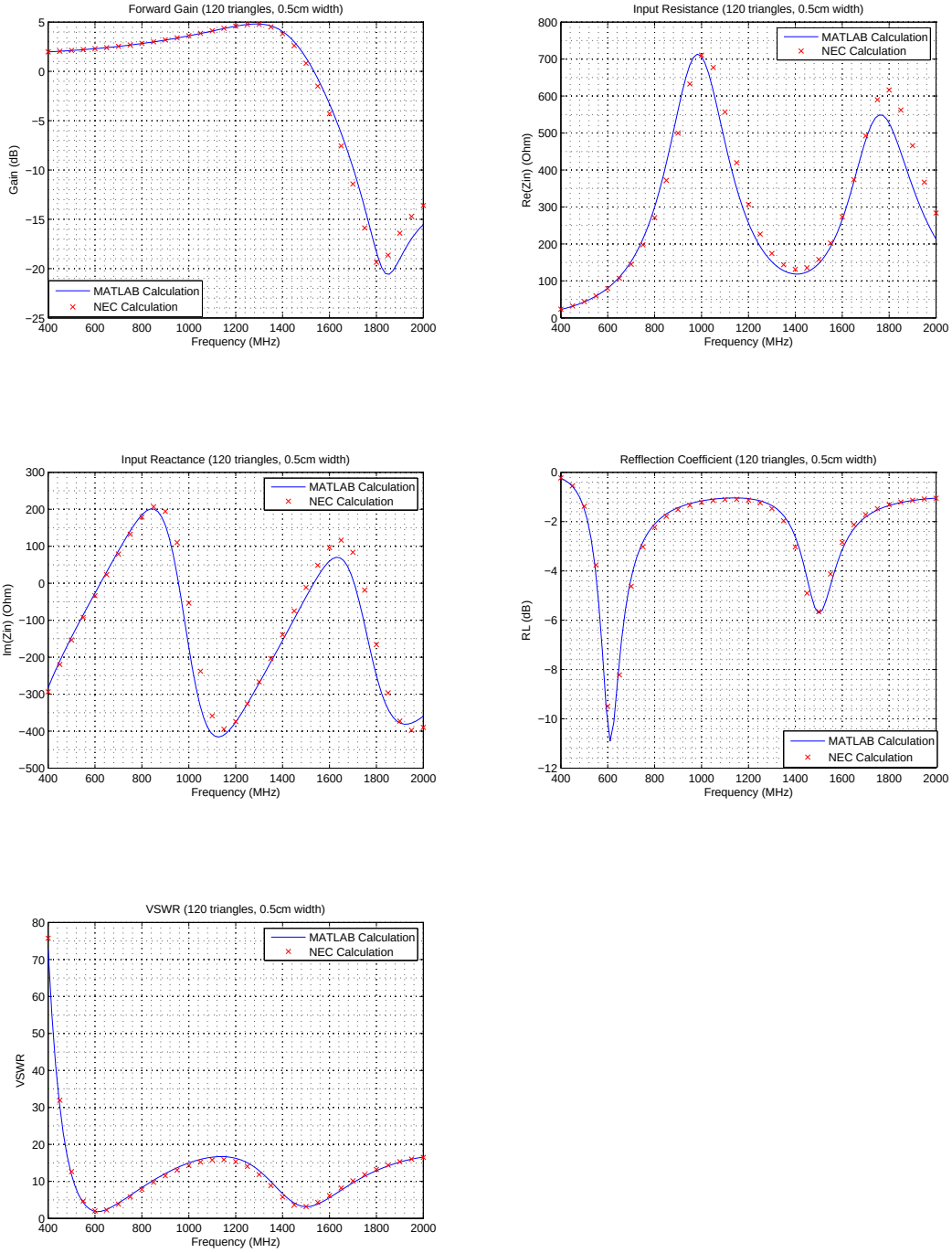

Figure 3.12: Capacitively Loaded Dipole Antenna; 2x1 pF at $l/4$ and $3l/4$

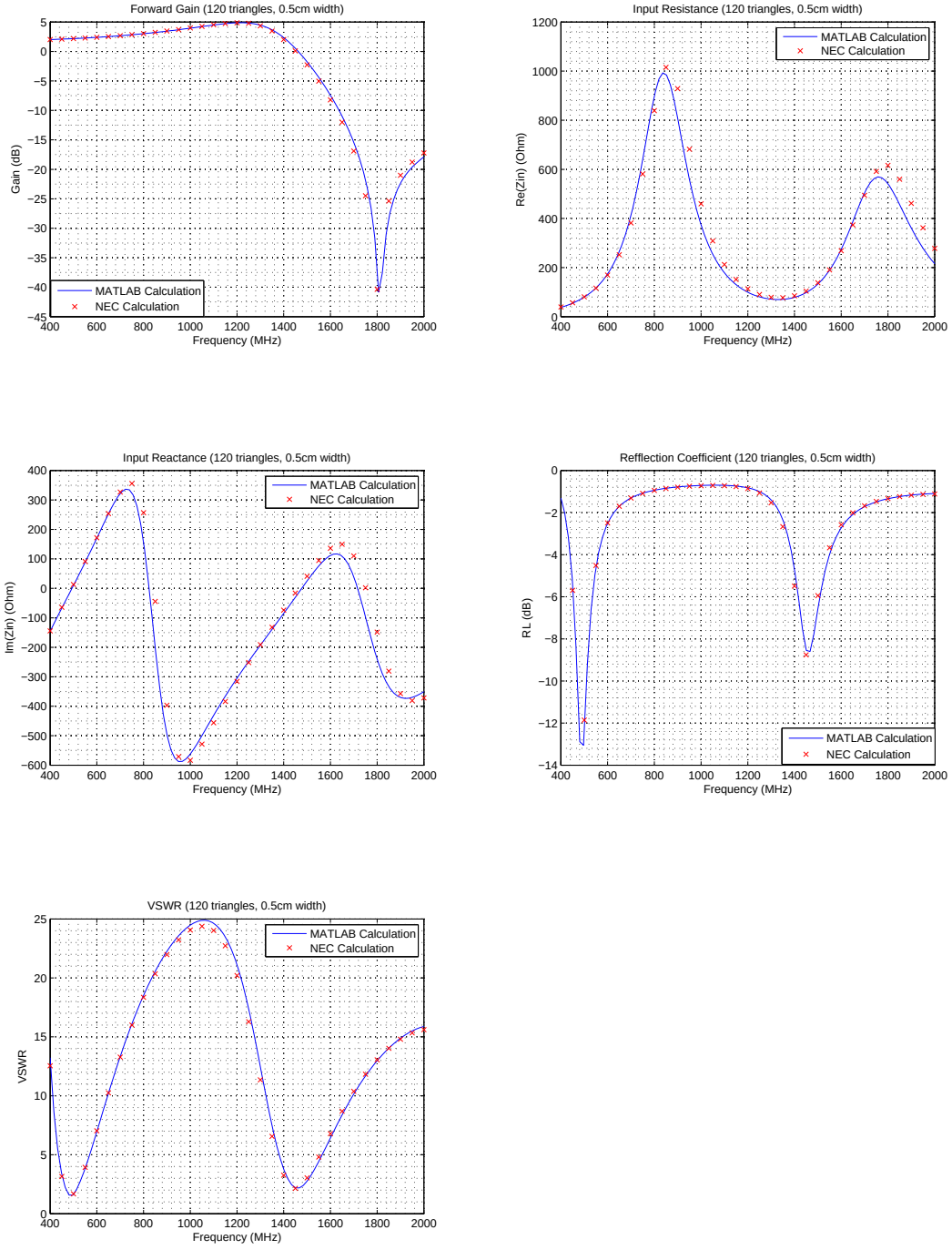

Figure 3.13: Capacitively Loaded Dipole Antenna; 2x10 pF at $l/4$ and $3l/4$

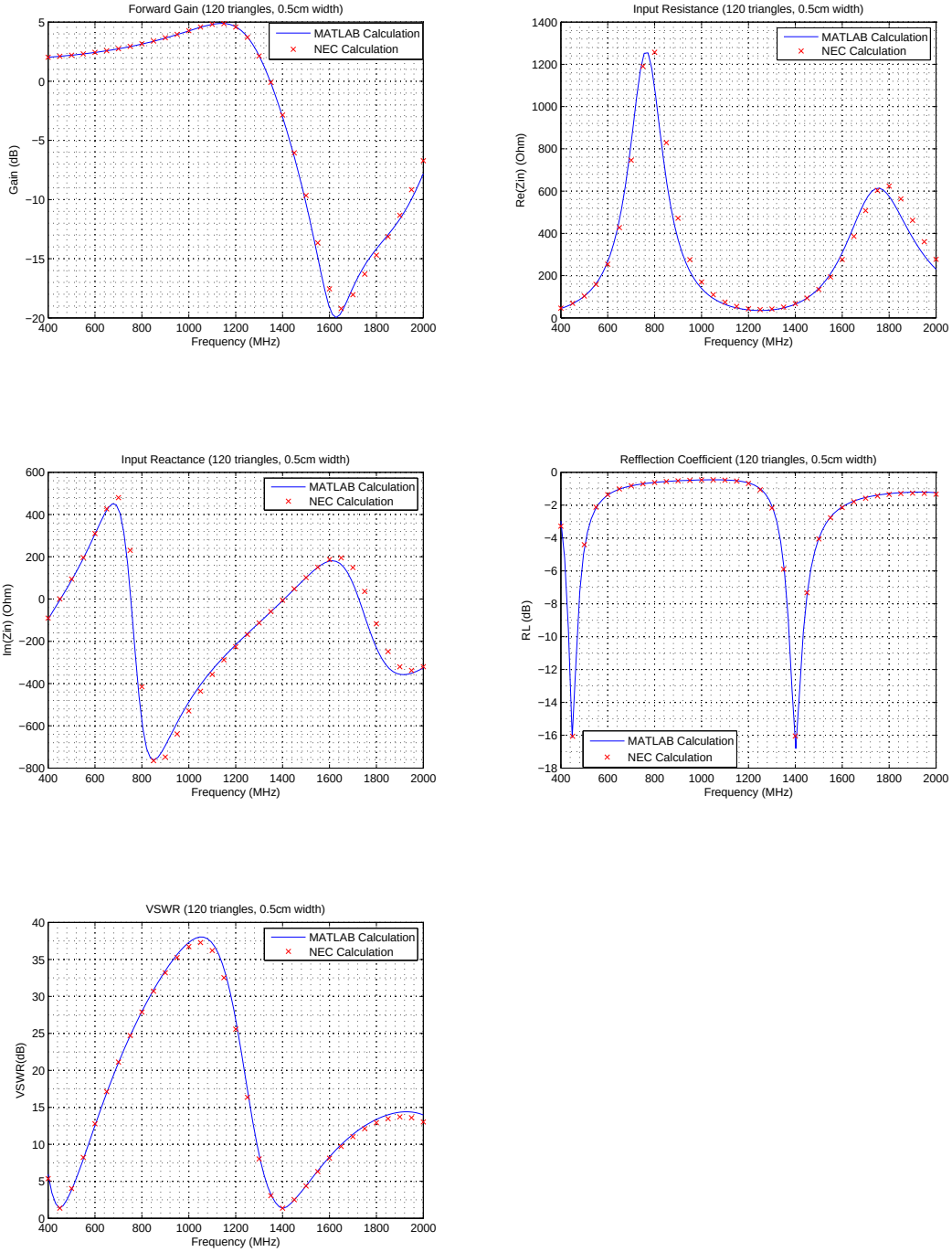

Figure 3.14: Inductively Loaded Dipole Antenna; 2x10 nH at $l/4$ and $3l/4$

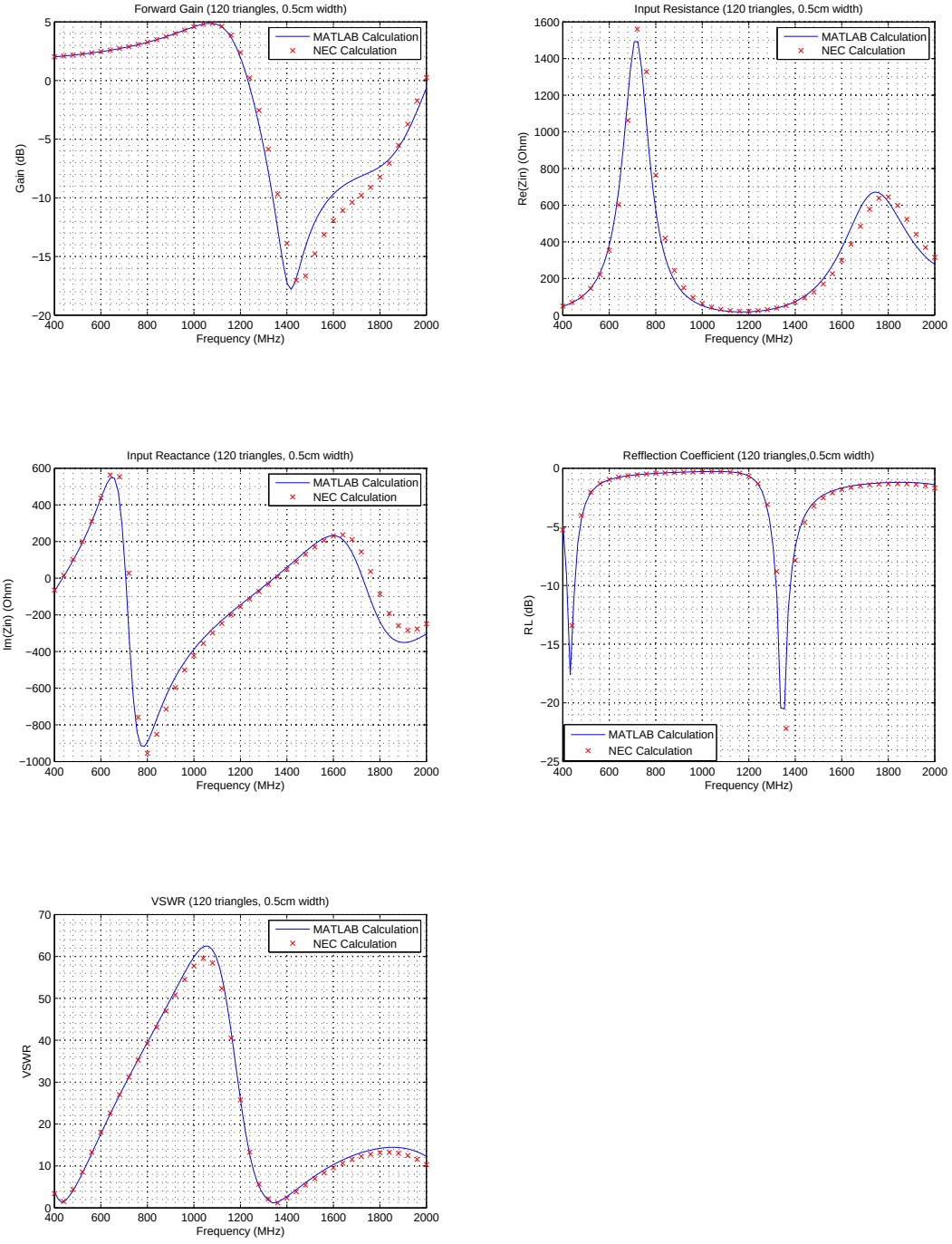

Figure 3.15: Inductively Loaded Dipole Antenna; 2x20 nH at $l/4$ and $3l/4$

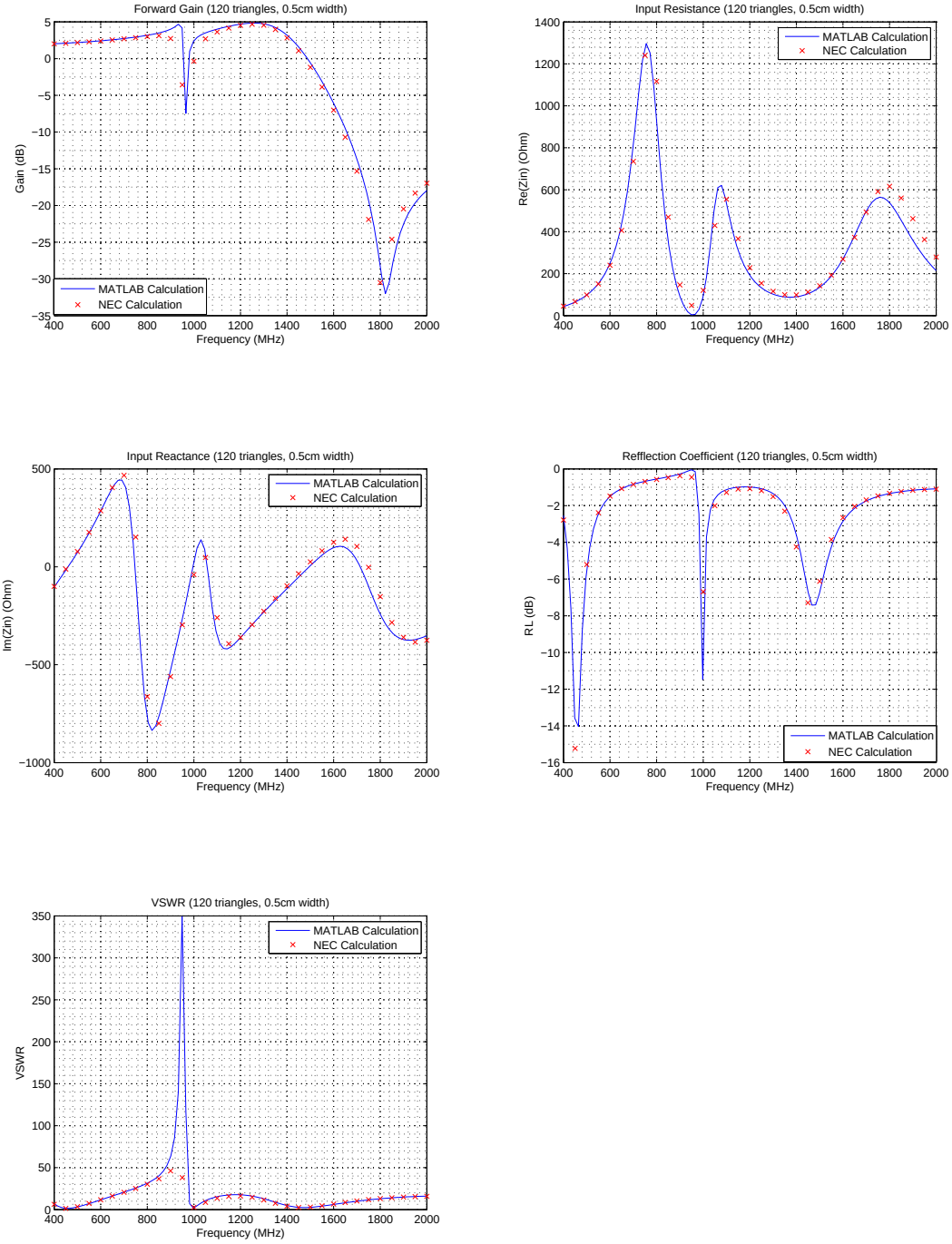

Figure 3.16: L-C Trap; 5 nH and 5 pF at $l/4$ and $3l/4$

CHAPTER 4

GENETIC ALGORITHM OPTIMIZATION OF LOADED DIPOLE

4.1 Genetic Algorithm Procedure

Genetic algorithm is an optimization method inspired by genetics theory of biology. Basically it relies on the assumption that, good parents will reproduce good individuals. Genetic algorithm optimization searches for global optimum by the use of natural selection, cross-over and the mutation operators.

Genetic algorithm procedure starts with the generation of an initial population (P_0) which consist of possible solutions of the optimization problem. Every possible solution in the population is named as a "chromosome". One chromosome should include all the features of the problem that are required to be optimized. Every single feature is called a "gene". After a population is generated, fitness of all chromosomes in the population are evaluated by the use of a cost function. Cost function calculates the amount of proximity of the result obtained to the targeted result. Then, according to the cost function results, some of the weak chromosomes are eliminated by "Natural Selection" (P_s). After the natural selection, survivors are matched by some selection methods to generate new offsprings by the use of "crossover" operator (P_c). Lastly, to prevent the optimization from stalling, mutation process, which means changing some properties of some chromosomes randomly, is implemented (P_m).

As a result, a new population is generated which is composed of mutated parents and new offsprings. Further generations are obtained by the same procedure

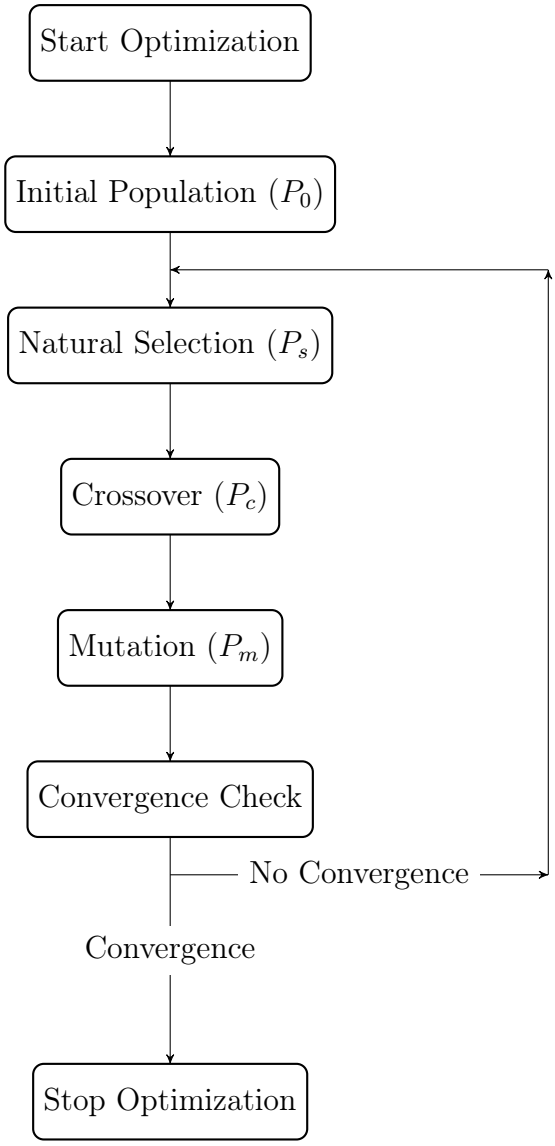

Figure 4.1: Genetic Algorithm Flowchart

until cost value drops below a target value. Flowchart is shown in Figure 4.1.

4.1.1 Chromosomes and Binary Encoding

Chromosomes are the individuals that are composed of genes. Every gene represents a solution to one feature that is required to be optimized and every chromosome is also a solution to whole problem. In most cases, binary representation is used to express the chromosomes since it provides easy implementation

of crossover and mutation operators. In an optimization problem, fitness of the chromosomes are calculated usually in decimal numbers however genetic algorithm is applied in binary domain. Therefore to use binary representation, a conversion should be defined between binary and decimal domains.

A conversion of binary representation to decimal number can be defined as

$$X = X_{min} + \frac{X_{max} - X_{min}}{2^{nbit} - 1} \sum_{n=0}^{nbit-1} b_n 2^n \tag{4.1}$$

where X_{min} and X_{max} are the minimum and the maximum limits of the variable and "$nbit$" is the bit length of the value. b_n are the bits of the binary representation of X, "$nbit$" bits string $b_0, \ldots, b_{nbit}$ [2].

As seen from (4.1), length of the binary representation and the limits of the variables specify the variable resolution, since space between minimum (X_{min}) and maximum (X_{max}) limits of the variable is divided into $2^{nbit} - 1$ pieces and variable can take values that are multiples of $\frac{X_{max} - X_{min}}{2^{nbit}-1}$.

Limits of the variables are defined based on the optimization problem. For example, to optimize a load position in a loaded dipole problem, maximum value that position of the load can take is the length of the antenna (l_0) while minimum point is very close to zero. Then the position gene limits are defined as $0 < Position < l_0$.

However, resolution of a variable should be decided according to the desired precision of that value. If change in the load position more than "n" cm results in appreciable difference, then "n" cm resolution is reasonable. According to the variable limits and the resolution, bit string length ($nbit$) is decided.

Chromosomes are produced by concatenating the binary representations of the genes. Then, length of the chromosome bit string is the sum of the gene bit strings in that chromosome.

For the antenna loading optimization problem, with parallel R-L-C circuit loads, and we allocate "N_R" bits for R value, "N_L" bits for L value and "N_C" bits for C value and "N_P" bits for the position of the load, and end up with a

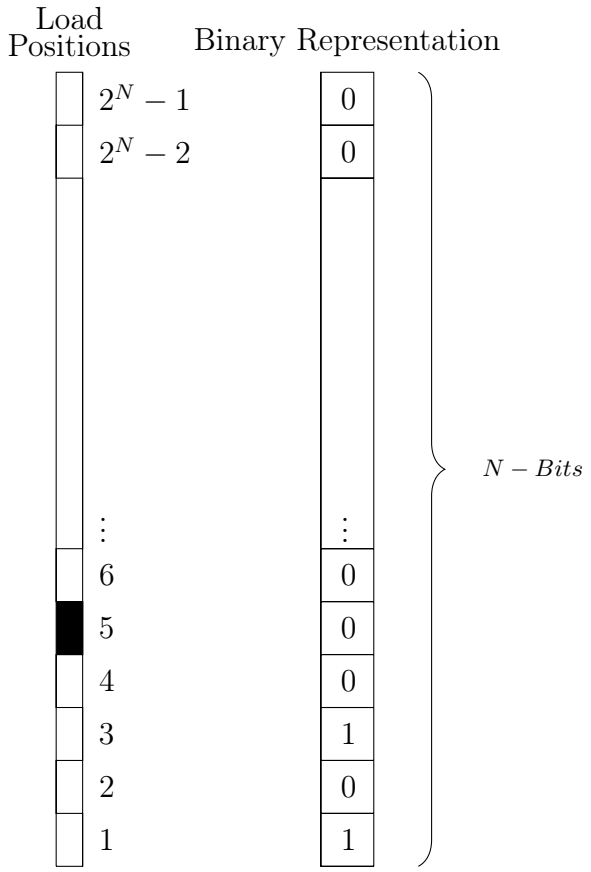

Figure 4.2: Load Position Binary Representation

$N = N_R + N_L + N_C + N_P$ bit chromosome.

For one lumped load situation, chromosome can be formed as:

$$Chromosome = \underbrace{1_R \ldots N_R}_{Gene_1:R-Value} \mid \underbrace{1_L \ldots N_L}_{Gene_2:L-Value} \mid \underbrace{1_C \ldots N_C}_{Gene_3:C-Value} \mid \underbrace{1_P \ldots N_P}_{Gene_4:Position} .$$

For antenna with "M" similar loads, chromosome length would be $M \times N$. Binary representation of this chromosome can be written as:

$$Chromosome = \underbrace{1 \ldots N}_{1_{st}-Load} \mid \underbrace{1 \ldots N}_{2_{nd}-Load} \mid \underbrace{1 \ldots N}_{3_{rd}-Load} \mid \cdots \mid \underbrace{1 \ldots N}_{M_{th}-Load} .$$

4.1.2 Initial Population

It would be beneficial to start with an initial population that contains all possible solutions in the search space. However, it is generally not possible to use such

a large population. Then, it would be desirable to have good individuals with high fitness values in the initial population. Generally, it is not possible to make a good initial estimation for optimal solution over the search space, and initial population is created randomly [21].

Number of the chromosomes in the population (n_{pop}) is an important parameter that should be specified by the user. Selecting population size larger provides solution space to be sampled in more detail and results in faster convergence to the solution. However, larger population size also requires more processing power and more data storage. Therefore, population size itself also needs to be optimized for different problems. Generally n_{pop} of around 100 is suggested ([21]).

One modified genetic algorithm method, named Micro-GA (Micro Genetic Algorithm) is proposed in [19] which requires really low number of population size (5 for the example in [19]). Mutation operator is not used in micro-GA and population is regenerated randomly after every 5 steps, except the healthiest chromosome. It is an alternative genetic algorithm method for users that don't want to use large population sizes.

4.1.3 Evaluation of Fitness

After the initial population is produced randomly, fitness of all chromosomes in the population are evaluated by the use of cost function. First, genes of the chromosome are separated since they were concatenated to form the chromosome. As an example, for a chromosome with 2 genes and both genes consisting of 4 bit strings, we can write:

Chromosome=[01011100]

Gene1=[0101], Gene2=[1100]

Then, every gene is converted to the decimal number by the use of (4.1) since cost function is defined in decimal numbers. Continuing the above example, we may assume that the maximum value of the variable as 15 and its minimum

value as 0, to obtain:

$$X = X_{min} + \frac{X_{max}-X_{min}}{2^{nbit}-1} \sum_{n=0}^{nbit-1} b_n 2^n$$
$$\text{Gene1} = 0 + \frac{15-0}{15}(1 \times 2^0 + 1 \times 2^2) = 5$$
$$\text{Gene2} = 0 + \frac{15-0}{15}(1 \times 2^2 + 1 \times 2^3) = 12$$

The value represented by "Gene-1" is 5 and "Gene-2" is 12. Then, fitness of the chromosomes are evaluated by using the cost function. A simple cost function can be defined as:

$$\text{Cost} : f(X_1 \dots X_n) = \sum_{k=1}^{n} {X_k}^2.$$

Then the cost for this chromosome is:

$$\text{Cost} = \sum_{k=1}^{2} {X_k}^2 = 5^2 + 3^2 = 34.$$

Cost function selection is the most important part of any optimization algorithm. Its choice should facilitate convergence to the global minimum. The result of the cost function represents the difference between the candidate solution and the optimal solution. This subject will be further investigated in Section (5.3).

In most cases, cost function is defined to incorporate more than one goal. As an example, requirements of an antenna design may be determined as maximizing the system gain while minimizing the VSWR. Such a problem is known as multiple-objective optimization. A common way of dealing with multiple objectives is to normalize the cost of each objective weight and add the weighted costs to get a single cost function [7], i.e.,

$$Cost_{total} = \alpha * Cost_1 + \beta * Cost_2$$

where α and β are weights and $Cost_1$ and $Cost_2$ are the cost functions for system gain and VSWR.

4.1.4 Natural Selection and Mate Selection

Natural selection is a process which allows the healthiest members of the population to survive for the production of the next generation. Implementation is simply keeping the "n" healthiest chromosomes and discarding the rest. If one population consists of "m" chromosomes, healthiest "n" will survive and the other "$m - n$" will be discarded. This is the implementation of the genetic principle of "survival of the fittest". The next generation consists of these best chromosomes and the individuals which are generated from them by the use of crossover and mutation operators.

A mate selection method is required to choose parents of the new offsprings. Roulette wheel selection which is used in this thesis work is one of the most commonly used methods. Parents are selected in a random way but proportional to the fitness of the chromosomes. The aim of the roulette wheel selection is to select healthiest mates that will produce better offsprings.

The members that survive after natural selection are sorted according to their cost values. Then a probability of selection is assigned to every chromosome based on its rank in the sorted population for rank based probability. Every member will have different probabilities. If we have "n" members and "p_m" represents the probability of the m_{th} element in the rank and the chromosomes are sorted ascending order of fitness, the probability of the m_{th} element is

$$p_m = \frac{n - m + 1}{(1 + 2 + \cdots + n)}$$

For example, if "n" is 4, the probabilities are

$$\begin{aligned} p_1 &= 4/(1 + 2 + 3 + 4) = 0.4 = \%40 \\ p_2 &= 3/(1 + 2 + 3 + 4) = 0.3 = \%30 \\ p_3 &= 2/(1 + 2 + 3 + 4) = 0.2 = \%20 \\ p_4 &= 1/(1 + 2 + 3 + 4) = 0.1 = \%10 \end{aligned} \tag{4.2}$$

In roulette wheel selection, a wheel is assumed that has the names of each chromosome written on it [7]. Every chromosome covers a segment proportional

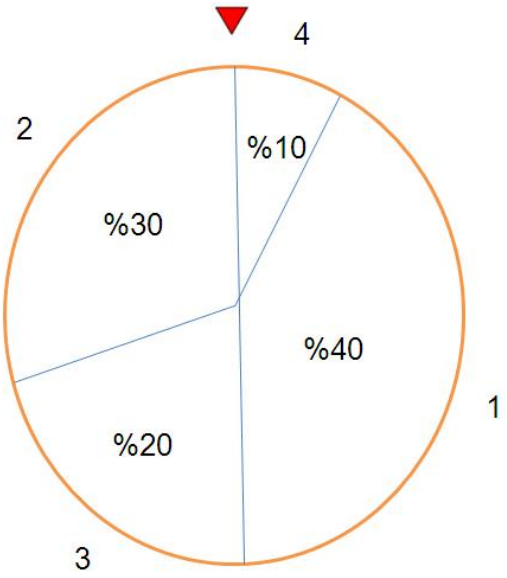

Figure 4.3: Roulette Wheel Selection

to its probability (p_n), which is calculated in (4.2). Wheel is rotated and when it stops, the chromosome that the arrow of the system points at is selected. Since we need a pair to have an offspring, wheel is rotated twice for each matching.

To implement roulette wheel selection, a random number "r" between 0 and 1 is generated. The chromosomes are located on the wheel to cover the range from 0 to 1, based on their probabilities as:

$$\begin{aligned} chromosome1 &= 0 \leq r \leq 0.4 \\ chromosome2 &= 0.4 < r \leq 0.7 \\ chromosome3 &= 0.7 < r \leq 0.9 \\ chromosome4 &= 0.9 < r \leq 1.0 \end{aligned}$$

Another type of roulette wheel selection can be defined where probabilities are specified according to the cost of the chromosomes. Then the probability of the m_{th} chromosome is;

$$\frac{Cost_m}{(Cost_1 + Cost_2 + \cdots + Cost_n)}$$

where "n" is the number of the selected members. However this type of selection is rarely used since it causes close valued chromosomes to have close probabilities.

4.1.5 Crossover and Offspring Generation

Crossover operator generates new offsprings from the chosen mates which are selected by the roulette wheel selection. Single point crossover, which is implemented in this study, is the process of generating two offsprings by combining two selected parents. If two selected chromosomes, called as mother and father, are "n" bit strings; a random number "r" is generated, which is between 0 and "n". First offspring is the combination of $[1 \dots r]$ bits of mother chromosome and $[(r+1) \dots n]$ bits of father chromosome. Second offspring is the reverse of first one, $[1 \dots r]$ bits of father chromosome and $[(r+1) \dots n]$ bits of mother chromosome.

To implement this type of crossover, mask generation is used. After "r" is determined, two masks are generated:

$$Mask1 = [\underbrace{111\dots1}_{\text{1 to r}} | \underbrace{000\dots0}_{\text{(r+1) to n}}]$$

$$Mask2 = [\underbrace{000\dots0}_{\text{1 to r}} | \underbrace{111\dots1}_{\text{(r+1) to n}}]$$

and offsprings can be defined by the use of these masks:

$$Offspring1 = Mask1 \times Mother + Mask2 \times Father$$
$$Offspring2 = Mask1 \times Father + Mask2 \times Mother$$

As an example, if chromosomes are 16 bit strings and random number "r" is 10, then we would get:

$$mother = [\underline{\underline{1001011010}}|\underline{001011}]$$
$$father = [\underline{0011101000}|\underline{\underline{100110}}]$$
$$Offspring1 = [\underbrace{1001011010}_{mother} | \underbrace{100110}_{father}]$$
$$Offspring2 = [\underbrace{0011101000}_{father} | \underbrace{001011}_{mother}]$$

The ratio of the chromosomes that are subjected to crossover operation, to the total chromosome number is called the "crossover rate". High crossover rate provides faster convergence to the optimal solution, although it may cause the fitter chromosomes to be lost sometimes. Crossover rate is suggested to be between 0.8 and 1 in [2] and between 0.6 and 0.8 in [15].

4.1.6 Mutation

Mutation operator is used to prevent optimization to converge to local optimal solution before the solution space is searched in detail. These local optima may cause the algorithm to stall and the global optimum can not be reached. Mutation induces random variations in the population. In binary representation mutation is implemented by simply, altering the bits in the population that are selected randomly.

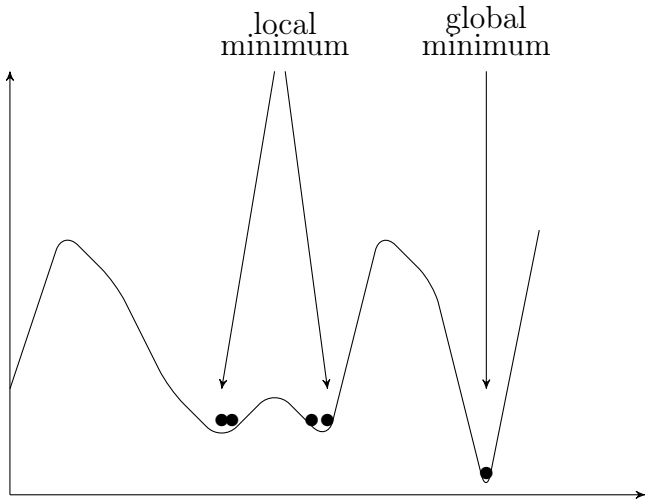

Figure 4.4: Mutation Operation

$$parent = [00\underline{1}1001\underline{0}11]$$
$$child = [00\underline{0}1001\underline{1}11]$$

If desired, healthiest chromosome can be excluded from mutation process. This ensures that the cost changes monotonically and prevents loosing the healthiest

chromosome.

Mutation rate is the ratio of bits that will be mutated to the total number of bits of the population. If it is selected too low, it won't make appreciable change; but if it is selected too high, it may cause divergence. Mutation rate between 0.0001 and 0.005 is recommended in [2], these suggestions are evaluated in the Section (5.2).

4.1.7 Termination of the Algorithm

The fittest element of the new generation is subjected to the convergence check after the mutation process. This is the last step of a single optimization cycle as shown in Figure (4.1). If the best chromosome satisfies the optimization requirements, algorithm is terminated; if not, cycle continues with natural selection.

Maximum generation number is added to the optimization algorithm as an additional control. In some optimization problems, results may not converge to the desired values because of the improperly selected predefined parameters. For these cases, a limit for maximum generation should be defined to terminate the algorithm, when generation number is reached to this limit.

CHAPTER 5

OPTIMIZATION EXAMPLES

In this chapter, several dipole antenna loading optimization examples are presented. Objectives of the optimization are selected as forward gain of the system (G_{sys}) and the VSWR. To calculate the fitness of the chromosomes, a computer program, based on the theory described in the second and third chapters are used. Moreover, a genetic algorithm code is developed and combined with this program to iteratively optimize loaded dipole antennas.

5.1 Predefined Parameters in the Problem

The length of the dipole is kept constant at 30 cm and optimization is carried over 2 different frequency ranges; namely, 400-1800 MHz and 400-2000 MHz. Requirements of the optimization are selected as maximum VSWR of 3.5 and minimum system gain of -3 dB.

Gain and VSWR behavior of the unloaded 30 cm length dipole is investigated in the Chapters 1 and 2. Therefore for the comparison of the results, data obtained in these chapters is used.

Dipole antenna is loaded with 3 parallel R-L-C circuits, and a matching network consisting of a transformer with turns ratio of "n" and a parallel inductance is considered. In one chromosome, there are 4 genes for each load. One gene for R value, one for L, one for C and one for the position of the load. Since we have 3 loads, there are 12 genes in a chromosome. With additional 2 genes, representing the turns ratio of transformer and the inductance value in the matching network,

total is 14 genes. If we use 7 bits for all variables, one chromosome is a $14 \times 7 = 98$ bit string.

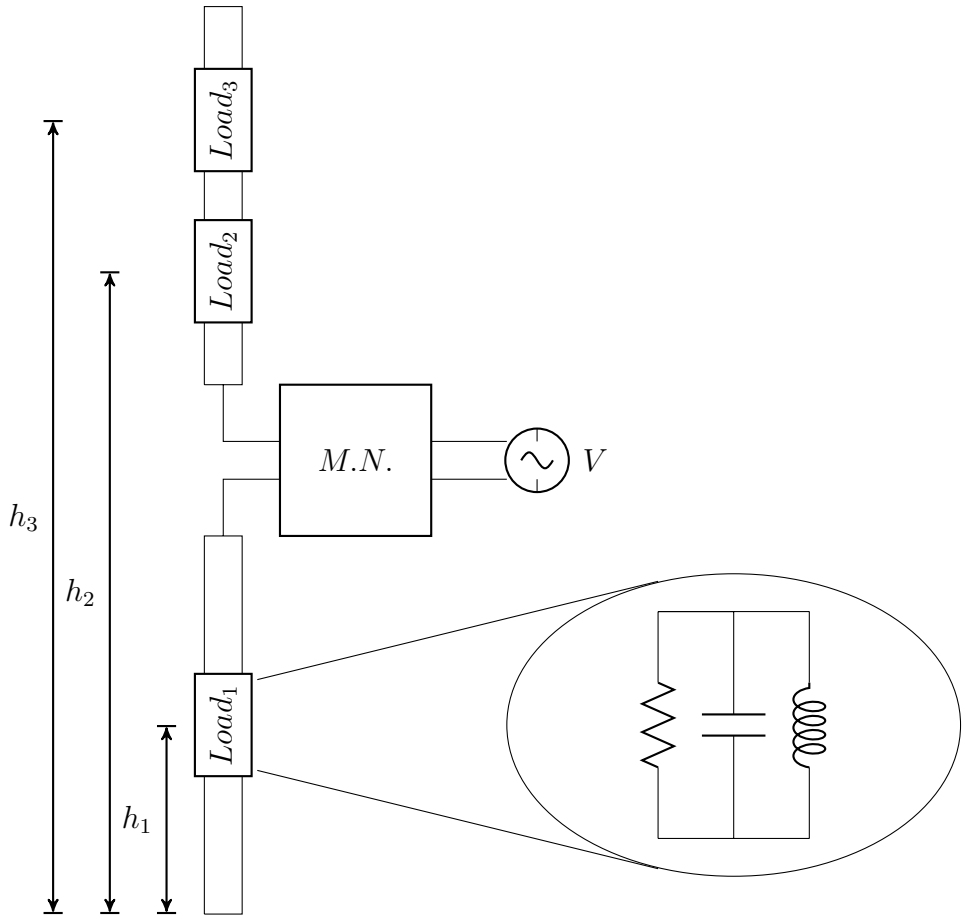

Figure 5.1: Optimized Antenna Structure

The limits for the variables are decided as following: $R = 0{-}5000\,\Omega$, $L = 0{-}5000$ nH, $C = 0 - 5000$ pF, $H(Position) = 0 - 30$ cm, $n(turnsratio) = 0.1 - 1$.

Since every variable is represented in 7 bits, resolutions are calculated as

$$Res_R = \frac{(R_{max} - R_{min})}{2^7 - 1} = 39.4\Omega$$

$$Res_L = \frac{(L_{max} - L_{min})}{2^7 - 1} = 39.4 \text{ nH}$$

$$Res_C = \frac{(C_{max} - C_{min})}{2^7 - 1} = 39.4 \text{ pF}$$

$$Res_H = \frac{(H_{max} - H_{min})}{2^7 - 1} = 2.3 \text{ mm}$$

$$Res_n = \frac{(n_{max} - n_{min})}{2^7 - 1} = 0.007$$

5.2 Genetic Algorithm Operators

Population size of 50, 100 and 200 are tried, 100 and 200 chromosomes gave acceptable results. After the natural selection, best 10 of chromosomes are survived. These 10 chromosomes are transferred directly to the new population. To generate new offsprings mates are selected by the use of "roulette wheel" selection. It was observed that, rank sorted and cost based probability assignments did not make much difference, and rank sorted probability assignment is used in optimization. Then, offsprings are generated by single point crossover. Point for the crossover is selected randomly. With new offsprings, number of chromosomes are raised to 100 or 200 again. Mutation is applied with a rate of "$nmut$". Mutation rate of 0.05 is found to be a good choice in our example, although it is higher than the recommendations. To keep the best individual, the best chromosome is not mutated.

5.3 Cost Function

Cost function contains the system gain and the VSWR. To satisfy the optimization requirements, the minimum system gain and the maximum VSWR over the

frequency band are considered. The cost function is defined as

$$Cost = \alpha F_g + \beta F_v$$

where F_g is the cost for the gain and F_v is the cost for VSWR and α, β are the coefficients. In the optimization examples that are presented below, values α=10 and β=1 are used and they gave acceptable results. The difference between obtained value and the desired value is normalized with the desired gain and VSWR:

$$F_v = \begin{cases} 0 & \text{, if } (VSWR)_{max} \leq V_0 \\ \frac{(VSWR)_{max} - V_0}{V_0} & \text{, otherwise} \end{cases} \tag{5.1}$$

$$F_g = \begin{cases} 0 & \text{, if } (G_{sys})_{min} \geq G_0 \\ \frac{G_0 - (G_{sys})_{min}}{G_0} & \text{, otherwise} \end{cases} \tag{5.2}$$

where G_0 is the target system gain of -3 dB and V_0 is the target VSWR of 3.5 [5]. System gain, (G_{sys}) or the absolute gain, (G_{abs}) is defined in Section (2.2.4.8).

$$G_{sys} = \underbrace{(1 - |\Gamma|^2)}_{ReflectionEfficiency} \underbrace{G(\theta = 90, \Phi)}_{AntennaGain}$$

By the use of genetic algorithm optimization, cost is decreased in each generation, where system gain is maximized and VSWR is minimized as shown in Figure (5.2).

Antenna gain, $(G(\theta = 90, \Phi))$ can be used instead of system gain in the cost function. However, since G_{sys} includes both effects of VSWR and the antenna gain and it is proportional to the amount of power that is transferred from transmission line to the observation point, we used G_{sys}. Antenna forward gain information is also given in the optimization example results for comparison.

5.4 Impedance Matrix Manipulation

Since genetic algorithm optimization is an iterative process, it has high computational cost. For one frequency sweep with 100 steps, impedance matrix should

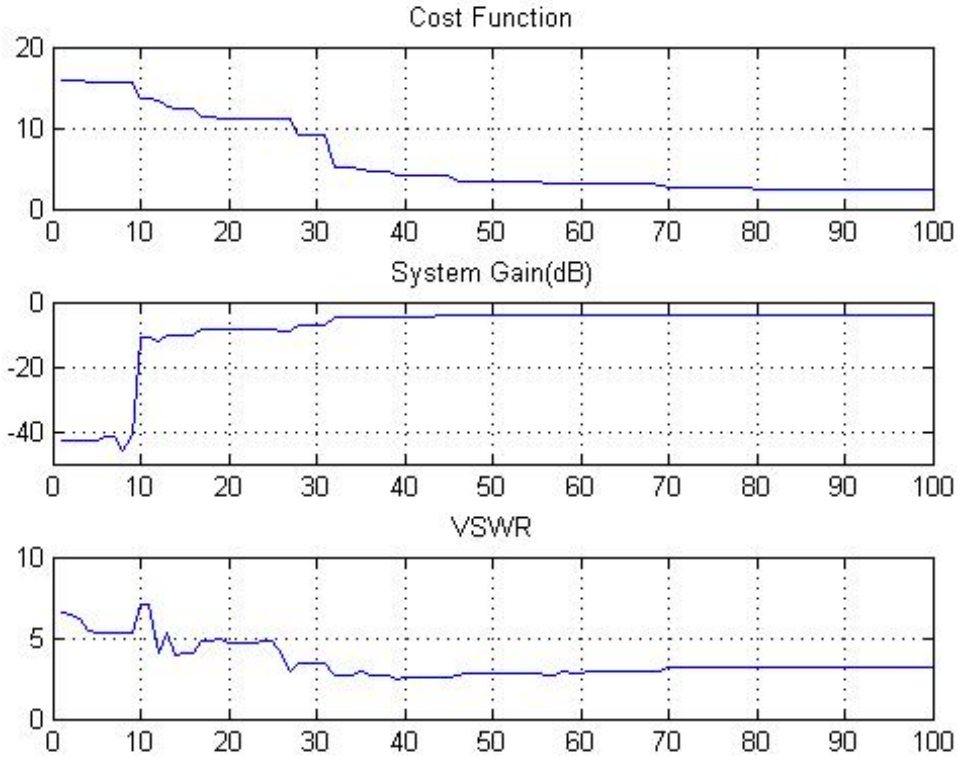

Figure 5.2: Genetic Algorithm Optimization

be calculated 100 times. During the optimization process, since we have 100-200 elements in the population, to find out the maximum gain and minimum VSWR over the band, all calculations must be done 10000-20000 times for each generation.

A method to decrease computational burden, based on Sherman, Morrison, Woodbury matrix inversion lemma is described in [2]. In this approach, the large MoM impedance matrix of the unloaded dipole is inverted only once for each frequency. As discussed in Section (3.1), MoM impedance matrix can be written as $Z = (Z^L + Z^0)$, where Z^0 is the unloaded impedance matrix and Z^L is a diagonal matrix determined by the R-L-C loads. We know that Z^0 changes only with the frequency and loading effects are expressed in Z^L. Then, we don't need to calculate Z_0 for every optimization cycle. It can be calculated for all frequencies for once and then only Z^L will be calculated for different load com-

binations. Since Z^L has only m (number of loads, which is chosen to be 3 in this work) non-zero components, computational load decreases drastically, [2]. In MATLAB code, calculation of the cost function can be done in 10 seconds for a population of 200 members, by the use of this method.

5.5 Evaluation of the Results

Three broadband dipole antennas obtained by the use of genetic algorithm optimization technique, are described in this section.

First optimization is done for a dipole antenna with 4.5:1 bandwidth, operating over 400-1800 MHz frequency range. Antenna is optimized successfully. Optimization results are shown in Figure (5.4) with the resultant configuration and results without matching network are shown in Figure (5.3). Algorithm resulted in two R-L and one R-L-C loads. Minimum system gain is higher than -2.5 dB and maximum VSWR is lower than 3.2. System gain was increased considerably except the first resonance frequency with respect to the unloaded antenna.

Minimum antenna forward gain is also presented. If we compare the resultant forward antenna gain with the unloaded dipole antenna forward gain, that is discussed in Section (3.3.4), decrease in the loaded antenna gain on overall frequency band is seen. The reason of the low forward gain is the losses due to the loading. Loads on the antenna dissipated some of the power and prevented the radiation of some antenna input power. Figure (5.5) compares the input power to the radiated power. If the loss due to the loads are added to the radiated power (where this summation is named as total power and shown by "x" in graph), it is seen that input power is exactly equal to the total power (total power and the input power drawings are overlapping). Therefore it is clear that the difference of the radiated power and input power is completely caused by the loading loss. This result shows that, antenna radiation efficiency is decreased while total power radiated to the observation point is increased over the band. This is an expected result whereas broadening the bandwidth can be achieved by loading with additional load losses. Moreover, directivity pattern of the an-

tenna is also shown in Figure (5.5). It is seen that although gain of the antenna is decreased, it is still directive in the forward direction.

Second optimization example is done for 5:1 bandwidth dipole operating over 400-2000 MHz. Algorithm resulted the optimized parameters shown in Figure (5.6) and (5.7). Resultant loads were two R-L and one R-L-C circuits. Minimum system gain of -2.9 dB and maximum VSWR of 3.2 are obtained. Loss due to the loading and the directivity vs gain comparison are shown in Figure (5.8).

Finally one more dipole antenna with bandwidth of 5:1 over 400-2000 MHz is designed. Acceptable results are taken and shown in Figures (5.9), (5.10) and (5.11). Maximum VSWR was less than 3.5 over most of the band and minimum system gain was 2.8 dB. These loaded antennas demonstrated good system gain especially at the frequencies (1800 MHz) where unloaded antenna has null as shown in Figure (5.12).

Loads	Resistance(Ω)	Inductance(nH)	Capacitance(pF)	Position(cm)
1	4724	3543	0	4.5
2	2087	157	0	28.3
3	472	157	2559	18.5
L_m	118 nH			
n	0.36			

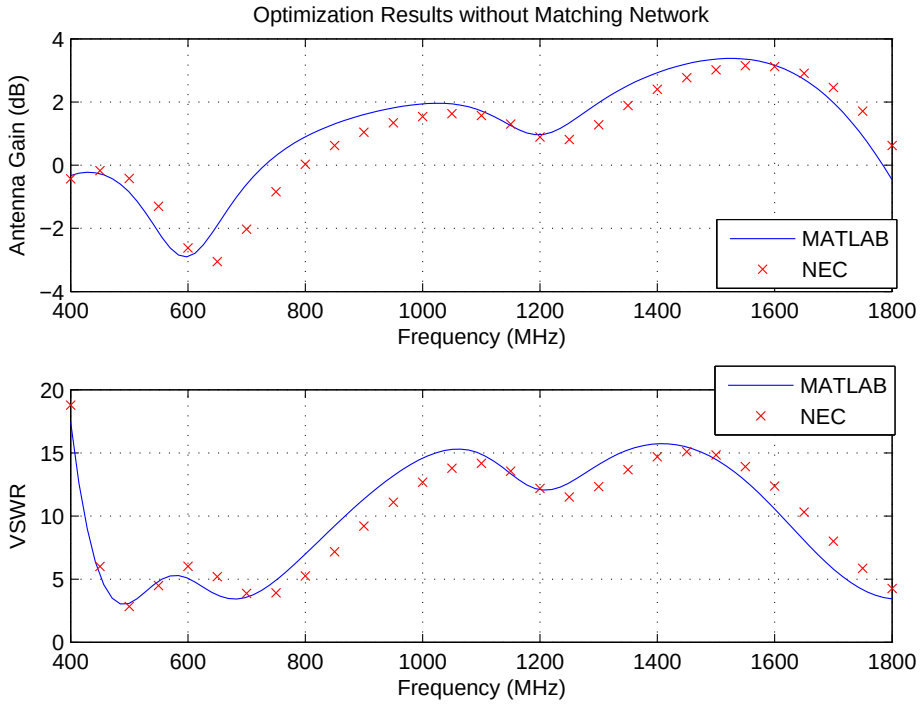

Figure 5.3: Optimized Dipole-1 without Matching Network

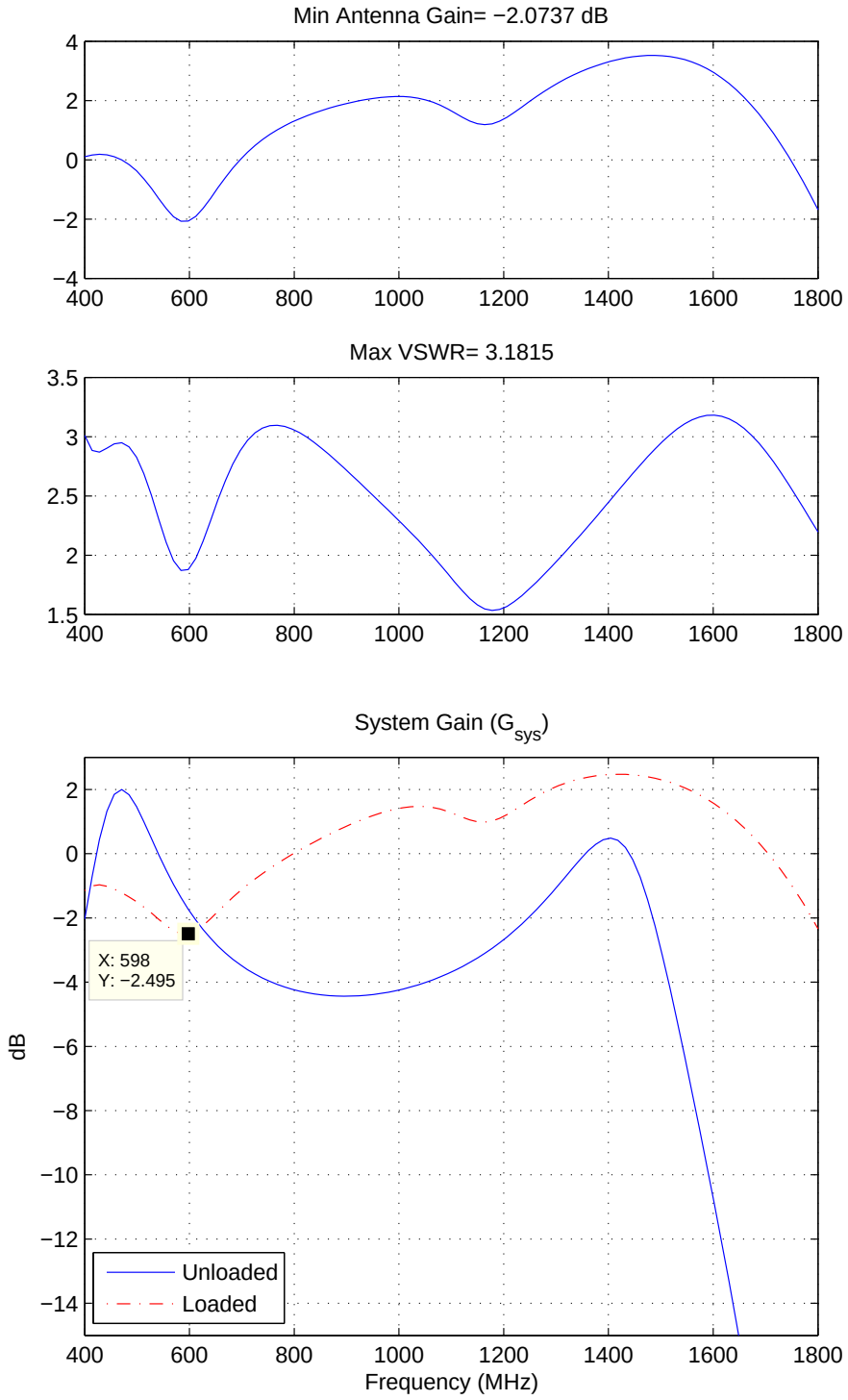

Figure 5.4: Optimized Dipole-1 at 400-1800 MHz

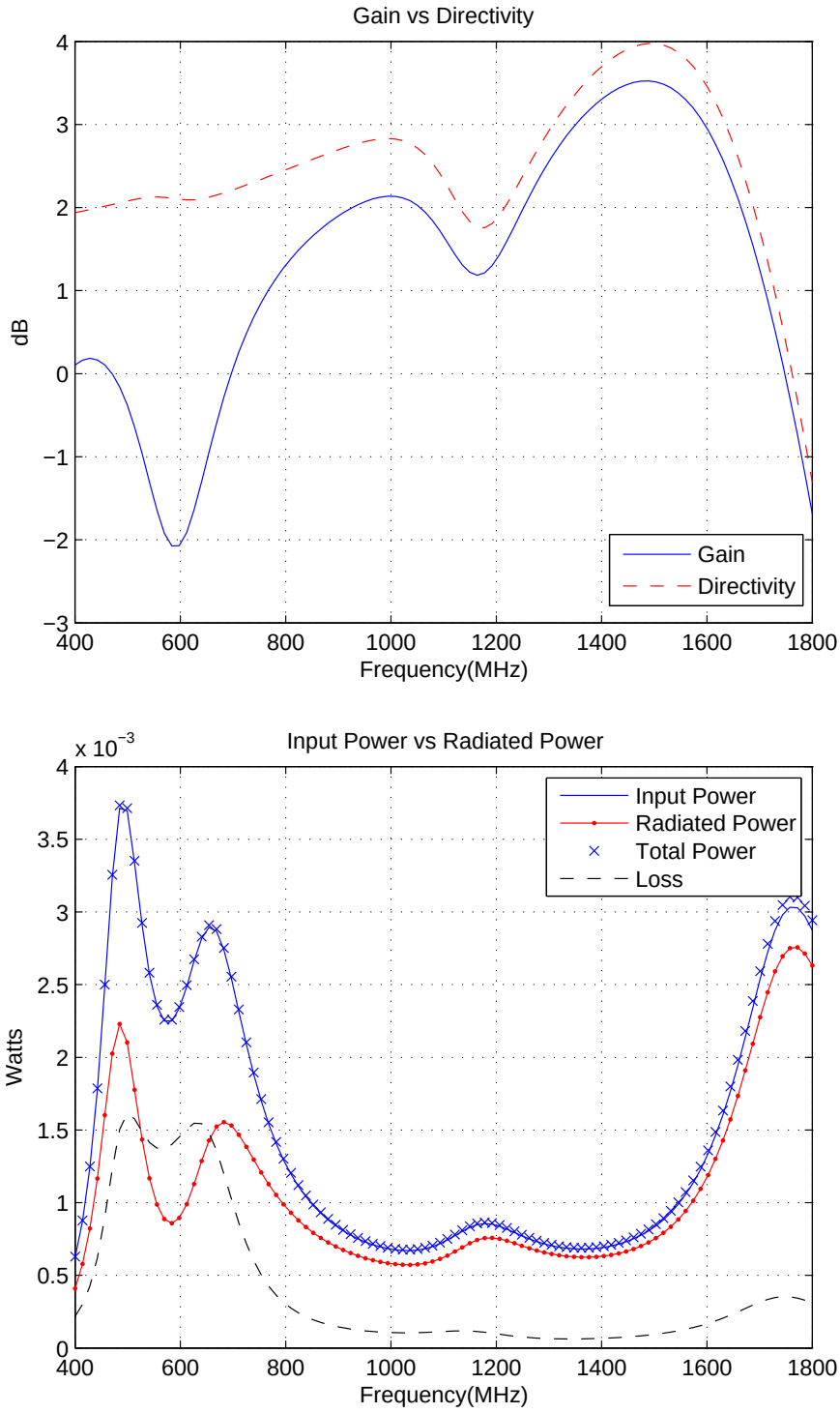

Figure 5.5: Optimized Dipole-1

Loads	Resistance(Ω)	Inductance(nH)	Capacitance(pF)	Position(cm)
1	2323	3583	0	4.7
2	472	39	0	25.5
3	1614	3622	669	15.2
L_m	157 nH			
n	0.38			

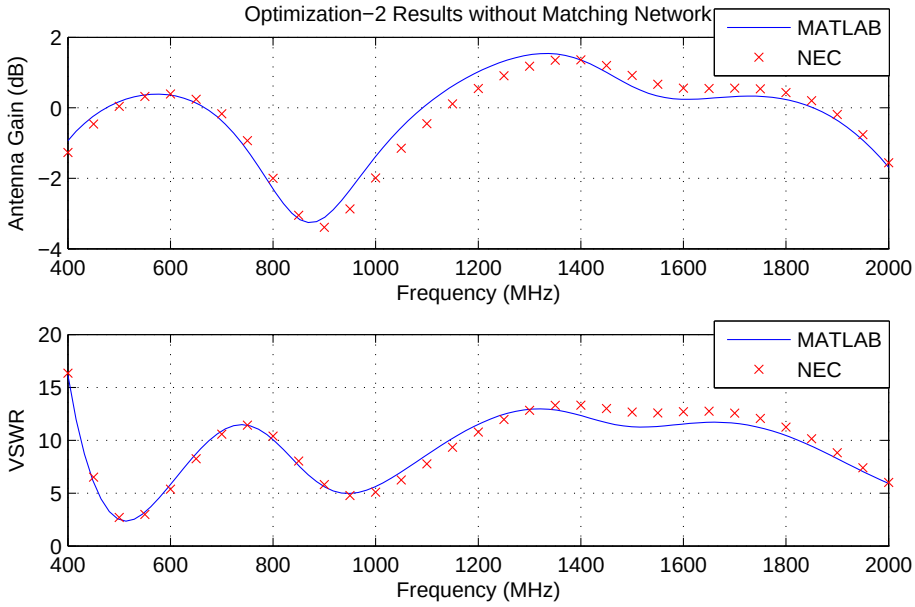

Figure 5.6: Optimized Dipole-2 without Matching Network

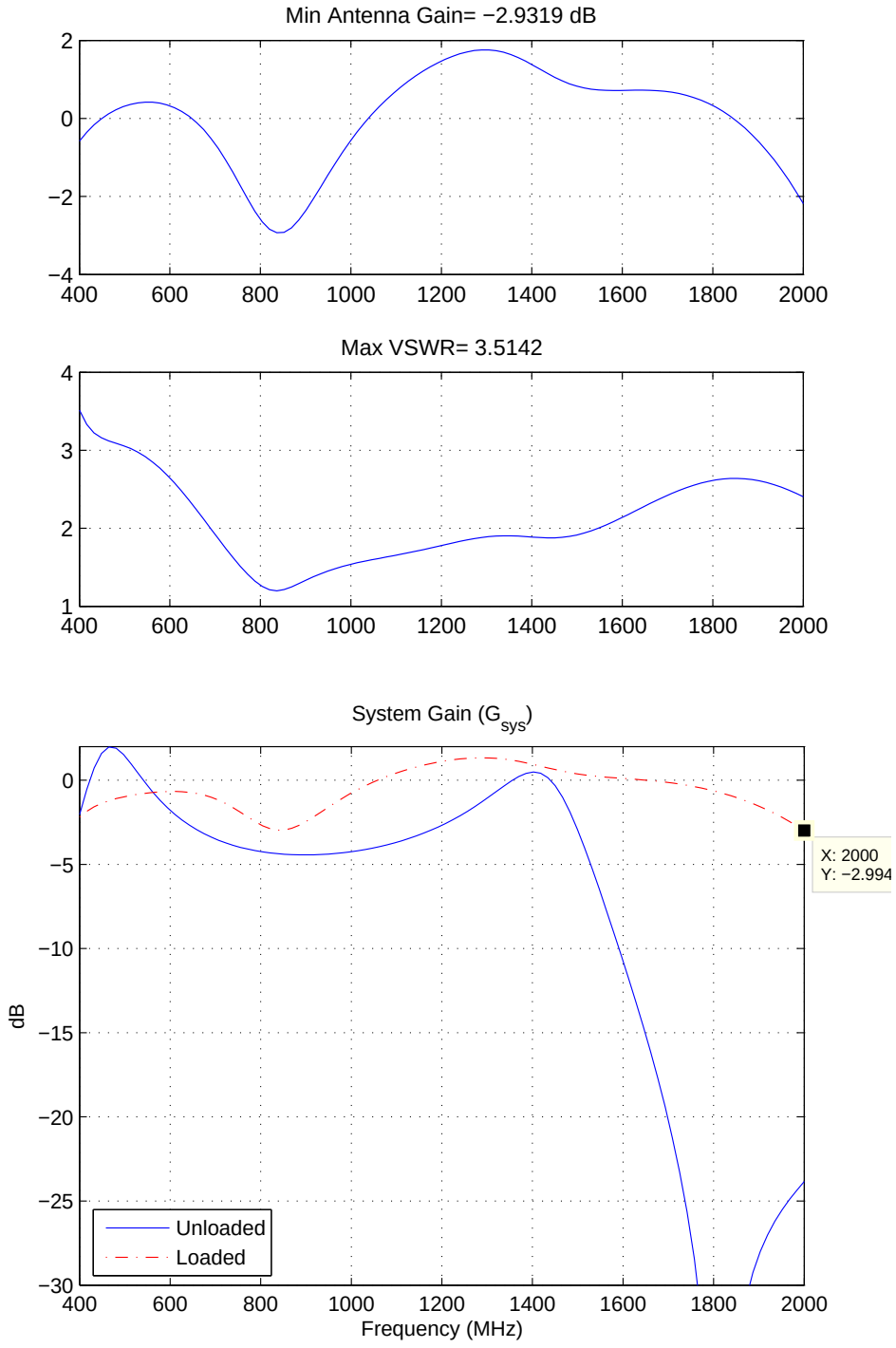

Figure 5.7: Optimized Dipole-2 at 400-2000 MHz

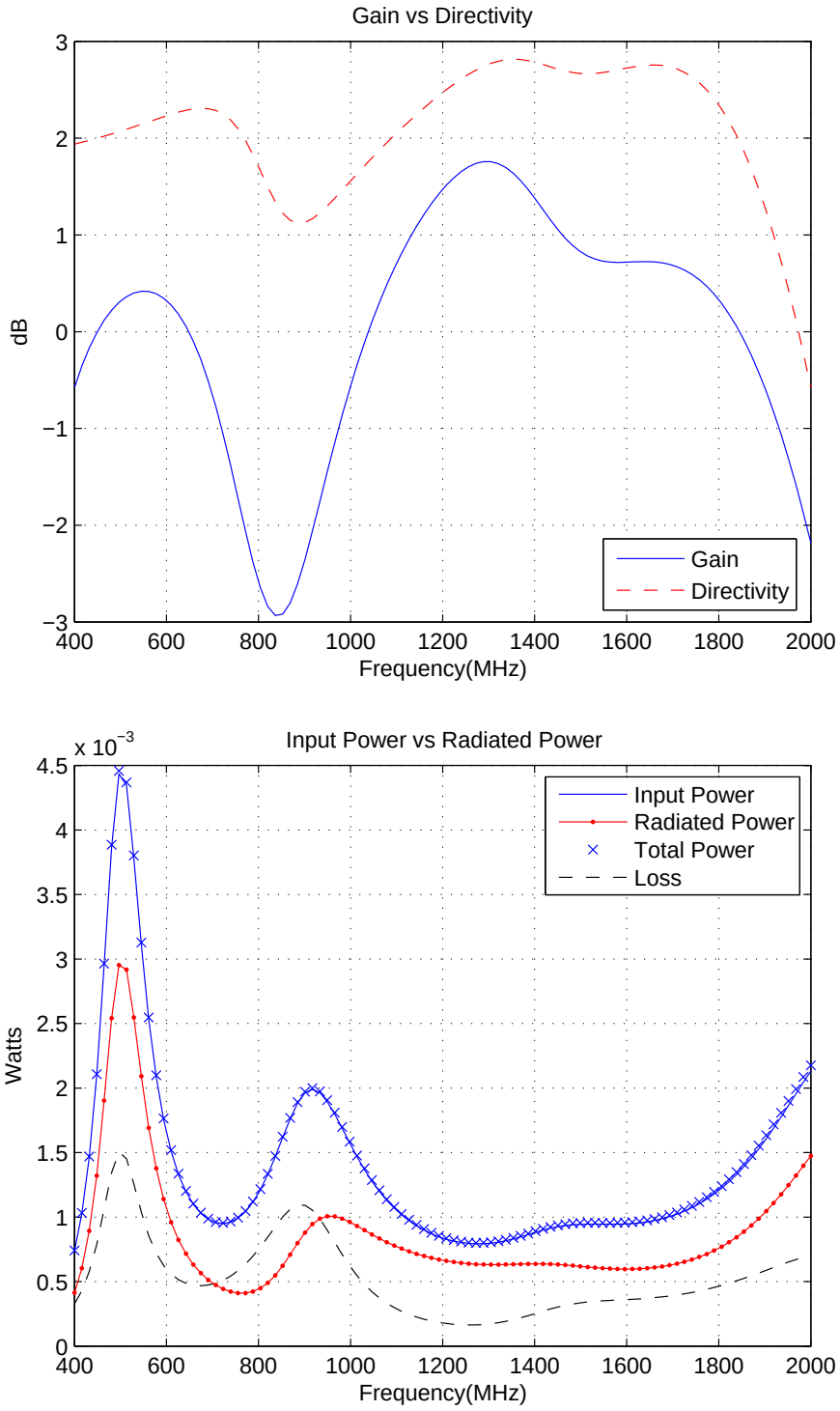

Figure 5.8: Optimized Dipole-2

Loads	Resistance(Ω)	Inductance(nH)	Capacitance(pF)	Position(cm)
1	5000	4882	0	25.5
2	4961	4961	0	3.1
3	2874	118	0	24.6
L_m	156 nH			
n	0.4			

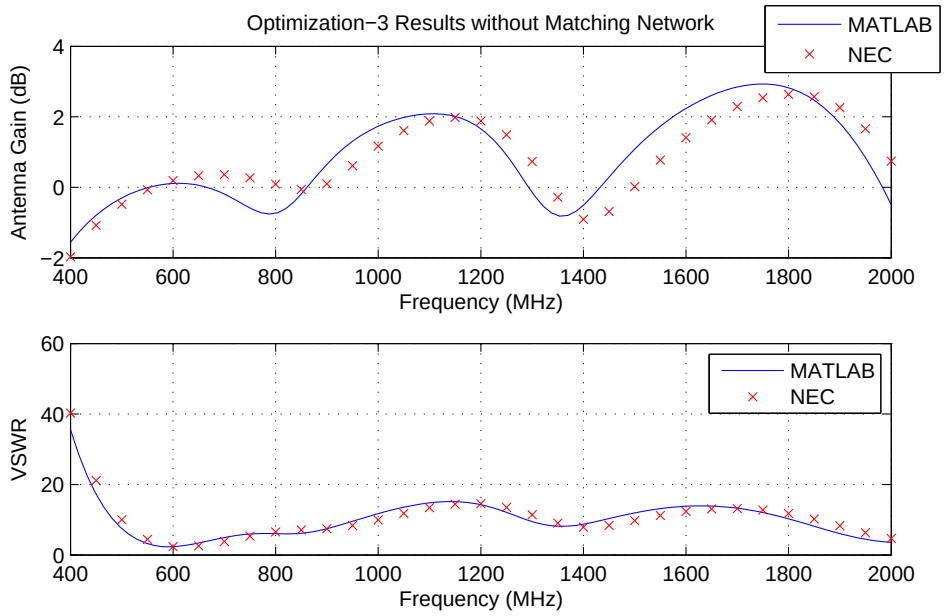

Figure 5.9: Optimized Dipole-3 without Matching Network

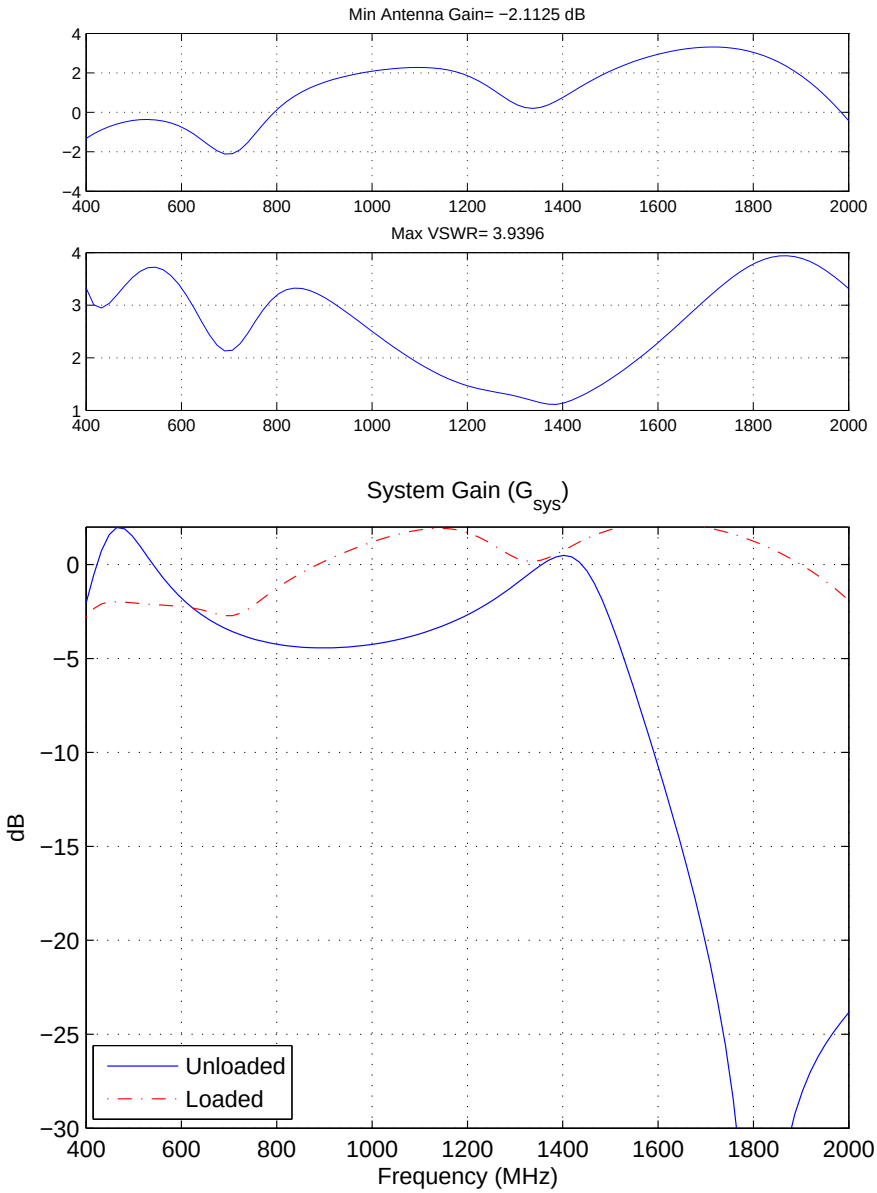

Figure 5.10: Optimized Dipole-3 at 400-2000 MHz

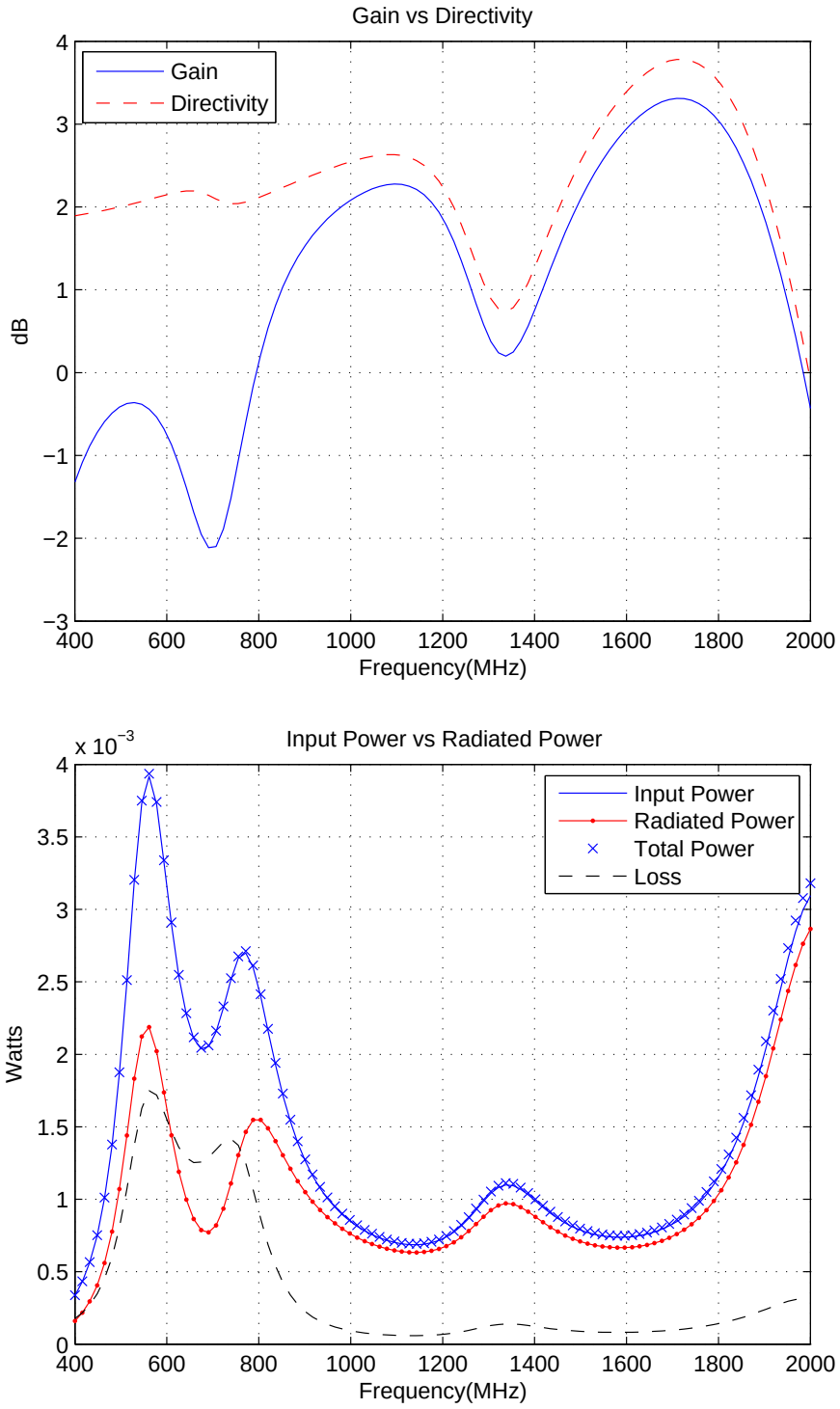

Figure 5.11: Optimized Dipole-3

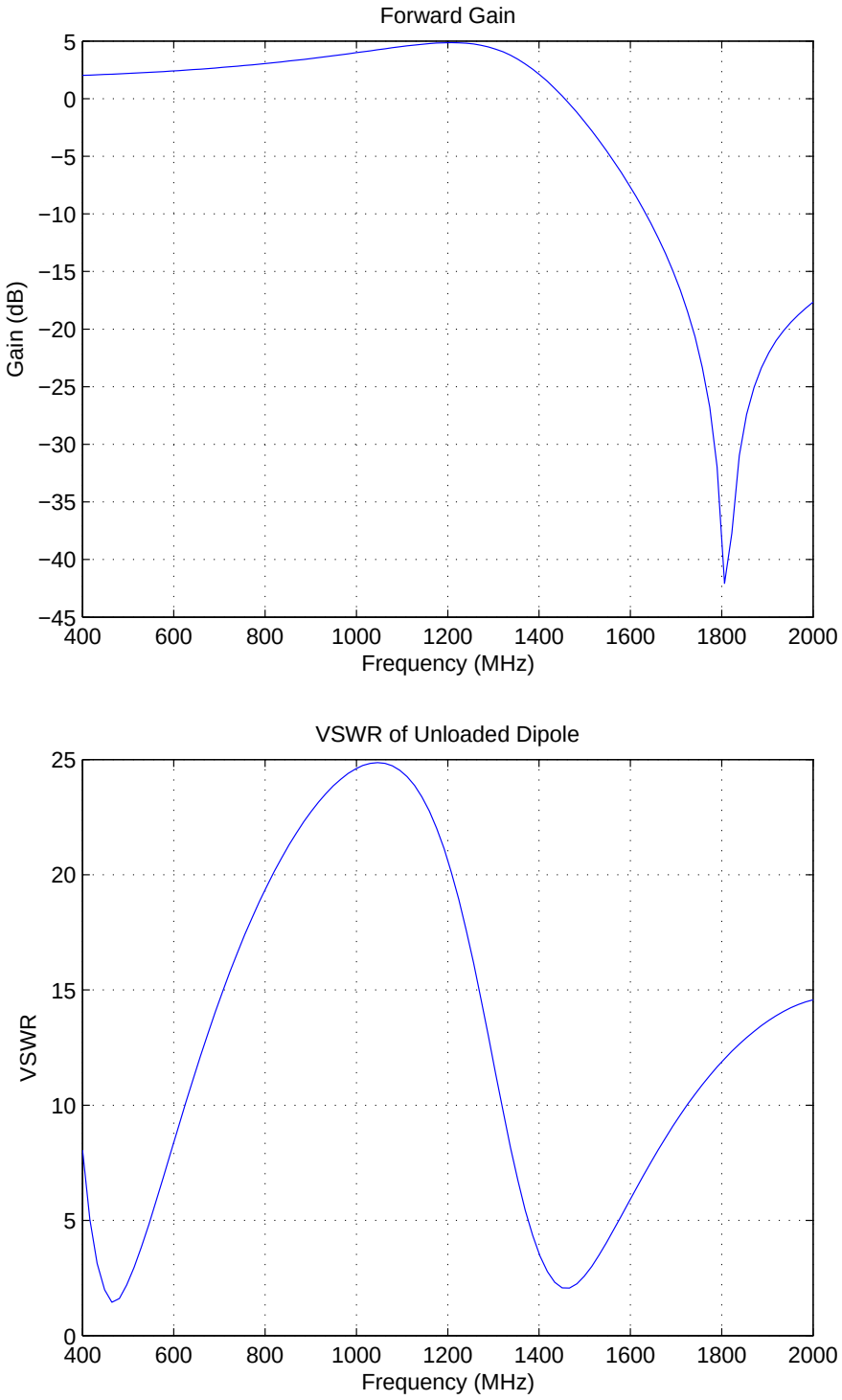

Figure 5.12: Unloaded Dipole

CHAPTER 6

CONCLUSION AND FUTURE WORK

6.1 Conclusion

In this thesis work, a procedure for broadband loaded dipole antenna design is presented. As a starting point, EFIE derivation for unloaded and loaded dipole antenna is provided for dipole antenna analysis. Then a "Genetic Algorithm" based optimization method to design broadband dipole antennas with low VSWR and high gain is discussed.

Genetic algorithm has been used in loaded wire antenna designs for years. A loaded wire antenna design by the use of genetic algorithm was done by Rogers to achieve 5:1 bandwidth over 200-1000 MHz, with VSWR less than 3.5 and system gain greater than -4 dB [18]. In a similar study, 20:1 bandwidth wire antenna design is achieved with VSWR less then 3 and system gain greater then -3.2 dB [19]. A successful loaded wire antenna design is given in [2] between 30-450 MHz, where system gain and VSWR are required to be greater than 0 db and less than 3.5.

Monopole antennas were not studied in this work. However, since a monopole antenna, which is located on an infinitely large perfect conductor can be modeled as a dipole antenna by the use of "Image Theory", this analysis and optimization tool can also be used for loaded monopole antenna design.

In this work, three broadband dipole antennas of 30 cm length were designed with bandwidths 4.5:1 over 400-1800 MHz, 5:1 over 400-2000 MHz. All antennas

achieved the design goals of maximum 3.5 VSWR and minimum -3 dB system gain, over most of the design bandwidth.

It was investigated in the Section (5.5) that losses due to the loading caused forward antenna gain to decrease. It was found that, the ability to operate the antenna over a broadband with low VSWR comes at the expense of efficiency [18]. However, since VSWR was decreased in a considerable amount, power transferred to the antenna from transmission line is increased. This was shown by the increase of the system gain (G_{sys}), since it takes into account both the transmission line mismatch and the antenna gain. According to the Figures(5.4), (5.7) and (5.10); loading decreased the VSWR and increased the system gain in spite of causing additional losses.

For further investigation, dissipated power in the loads were calculated by the use of load impedance and the port current. It was then compared with the difference of radiated and input power. Although the gain of the antenna is decreased due to the power dissipated by the loads, they were still directive as shown in the "Directivity vs Antenna Gain" figures.

6.2 Future Work

This optimization process was designed to decrease maximum VSWR and to increase minimum system gain over a broad bandwidth. However in some applications, average gain and VSWR may be considered more important. Therefore, in addition to the to the maximum VSWR and minimum gain requirements, average gain and VSWR optimization can be included as an additional objective.

The antennas that were designed in this study were not realized. Since optimization resulted in arbitrary load values, which are not available commercially, these loads should be produced specially. Some similar studies are documented in [2] and [18]. Moreover, when resultant optimized load values are changed slightly, it is seen that results are not effected that much, although results are more sensitive to load position changes. Therefore, optimized load values can be modified to have more realizable load values which will give very close results.

Another alternative is using loads that are potentially realizable. However this time it will be hard to optimize the antenna since population size will decrease.

In conclusion, for further studies, optimization may be extended to form an array of loaded dipoles in order to have directive patterns for direction finding (DF) applications. This time array elements and spacings will need to be added to the optimized parameters. Genetic algorithm optimization samples exist in the literature for antenna array designs.

REFERENCES

[1] C. A. Balanis. *Antenna Theory: Analysis and Design.* John Wiley & Sons, 2012.

[2] A. Boag, E. Michielssen, and R. Mittra. Design of electrically loaded wire antennas using genetic algorithms. *Antennas and Propagation, IEEE Transactions on*, 44(5):687, 1996.

[3] G. Burke and A. Poggio. Numerical Electromagnetics Code NEC—Method of Moments, Part iii: User's Guide. *Lawrence Livermore National Laboratory*, (1), 1981.

[4] R. E. Collin. *Antennas and Radiowave Propagation*, volume 108. McGraw-Hill New York, 1985.

[5] X. Ding, B.-Z. Wang, G. Zheng, and X.-M. Li. Design and Realization of a GA-Optimized VHF/UHF Antenna With. *Antennas and Wireless Propagation Letters, IEEE*, 9:303–306, 2010.

[6] E. Hallén and R. Gåsström. *Electromagnetic Theory*, volume 43. Chapman & Hall London, 1962.

[7] R. L. Haupt and D. H. Werner. *Genetic Algorithms in Electromagnetics.* Wiley. com, 2007.

[8] M. Kanda. Time domain sensors for radiated impulsive measurements. *Antennas and Propagation, IEEE Transactions on*, 31(3):438–444, 1983.

[9] C. Leat, N. Shuley, and G. Stickley. Triangular-patch model of bowtie antennas: validation against Brown and Woodward. In *Microwaves, Antennas and Propagation, IEE Proceedings*, volume 145, pages 465–470. IET, 1998.

[10] S. Makarov. *Antenna and EM Modeling with MATLAB.* Wiley-interscience, 2002.

[11] T. P. Montoya and G. S. Smith. A study of pulse radiation from several broad-band loaded monopoles. *Antennas and Propagation, IEEE Transactions on*, 44(8):1172–1182, 1996.

[12] F. A. Pisano III and C. M. Butler. Methods for modeling wire antennas loaded with shielded networks. *Antennas and Propagation, IEEE Transactions on*, 52(4):961–968, 2004.

[13] D. Poljak and C. Y. Tham. *Integral Equation Techniques in Transient Electromagnetics*. WIT, 2003.

[14] B. Popovic, M. Dragovic, and A. Djordjevic. Analysis and synthesis of wire antennas. *Research Studies PressLetchworth*, 1982.

[15] Y. Rahmat-Samii and E. Michielssen. *Electromagnetic Optimization by Genetic Algorithms*. John Wiley & Sons, Inc., 1999.

[16] B. Rao, J. Ferris, and W. Zimmerian. Broadband characteristics of cylindrical antennas with exponentially tapered capacitive loading. *Antennas and Propagation, IEEE Transactions on*, 17(2):145–151, 1969.

[17] S. Rao, D. Wilton, and A. Glisson. Electromagnetic scattering by surfaces of arbitrary shape. *Antennas and Propagation, IEEE Transactions on*, 30(3):409–418, 1982.

[18] S. D. Rogers, C. M. Butler, and A. Q. Martin. Realization of a Genetic-Algorithm-Optimized wire antenna with 5:1 bandwidth. *Radio Science*, 36(6):1315–1325, 2001.

[19] S. D. Rogers, C. M. Butler, and A. Q. Martin. Design and realization of GA-optimized wire monopole and matching network with 20:1 bandwidth. *Antennas and Propagation, IEEE Transactions on*, 51(3):493–502, 2003.

[20] M. N. Sadiku. *Numerical Techniques in Electromagnetics*. CRC press, 2010.

[21] S. Sivanandam and S. Deepa. *Introduction to Genetic Algorithms*. Springer, 2007.

[22] W. L. Stutzman and W. A. Davis. *Antenna Theory*. Wiley Online Library, 1998.

[23] T. Wu and R. King. The cylindrical antenna with nonreflecting resistive loading. *Antennas and Propagation, IEEE Transactions on*, 13(3):369–373, 1965.